

**EXAMINATION OF THE JAHN-TELLER
PHYSICS OF NaNiO_2 AND LiNiO_2 USING
X-RAY ABSORPTION SPECTROSCOPY
AND CONFIGURATION INTERACTION**

By

ERIC ALLEN MILLS, B.Sc.

A Thesis

Submitted to the School of Graduate Studies
in Partial Fulfillment of the Requirements
for the Degree
Master of Science

McMaster University
Copyright by Eric Allen Mills, 2008.

MASTER OF SCIENCE (2008)
(Physics)

McMaster University
Hamilton, Ontario

TITLE: Examination of the Jahn-Teller physics of NaNiO_2 and LiNiO_2 using
x-ray absorption spectroscopy and configuration interaction

AUTHOR: Eric Allen Mills, B.Sc.(McMaster University)

SUPERVISOR: John Berlinsky

NUMBER OF PAGES: xi, 83

**EXAMINATION OF MnO_2 XAS USING CONFIGURATION
INTERACTION**

Abstract

This thesis examines available x-ray absorption spectroscopy (XAS) data for NiO, NaNiO₂, and LiNiO₂. The XAS examined is the Ni L-edge, $3d^n 2p^6 \rightarrow 3d^{n+1} 2p^5$. The experimental spectra are compared to spectra calculated using a configuration interaction approach. This approach reproduces the spectra accurately. The NaNiO₂ spectrum is shown to be sensitive to the Jahn-Teller distortion, while the LiNiO₂ spectrum is reproduced by a hybridized $d^7 - d^8$ state that explains the lack of Jahn-Teller distortion in LiNiO₂.

Acknowledgements

I would like to thank John Berlinsky and Catherine Kallin for being excellent supervisors. Also I would like to thank Bruce Gaulin, George Sawatzky, and David Hawthorn for their contributions to this thesis. Thanks to Phil, Mike, Allan, Prasanna, and Pat Clancy for entertaining and occasionally useful discussions. Most of all, I would like to thank Sara for her unceasing support and encouragement.

Contents

1	Introduction and Description of Problem	1
1.1	Statement of the Jahn-Teller Problem	1
1.2	Review of the Literature	2
2	Description of Materials and Measurement	7
2.1	Crystal Structure	7
2.2	Materials Synthesis and Measurement	9
3	Theory of Configuration Interaction	11
3.1	The Hamiltonian	11
3.2	The single particle matrix elements	13
3.2.1	The crystal field	14
3.2.2	Group Theory and the symmetry specific form for the crystal field	17
3.2.3	The Hopping terms	19
3.3	The two particle matrix elements	21
3.4	Calculating the Spectra	25
4	Results and Discussion	29
4.1	NiO	29
4.2	NaNiO ₂ - Describing the Jahn-Teller Distortion	33
4.3	LiNiO ₂ - Determining the Formal Valency	37
4.4	Comparison of NaNiO ₂ and LiNiO ₂	46
4.5	Future Work	51

5	Conclusions	55
A	The Ewald Sum	57
B	Detailed Ground State Information	63
B.1	NiO	63
B.2	NaNiO ₂	68
B.3	LiNiO ₂	72

List of Tables

2.1	Room temperature crystal parameters. The NaNiO_2 parameters were taken from [1], while LiNiO_2 was taken from [2]. Both are given in terms of the $C2/m$ structure.	9
3.1	Diagonal matrix elements for d^2	24
3.2	Diagonal matrix elements for d^3	24
4.1	Parameters obtained for NiO in this thesis, with comparison to parameters obtained by other groups on the same compound. All values given in eV.	30
4.2	Results of the Madelung sum calculation for NaNiO_2 . This symmetry here is lower than cubic, and the intra- e_g and t_{2g} splitting is of the same order as the inter- splitting. This calls into question the validity of the point charge model used in the Madelung sum	33
4.3	Parameters determined for NaNiO_2 by providing best fit between calculated and experimental spectrum	36
4.4	Best fit parameters for LiNiO_2	40

List of Figures

1.1	Schematic of the energy levels of the $3d$ Ni orbitals in NaNiO_2 . The crystal field splitting removes the lower three orbital, which are filled, leaving a single electron in a state degenerate in both spin and orbital degrees of freedom (left) which is broken below 480 K by the Jahn-Teller distortion (right).	2
2.1	Crystal structure of MNiO_2 , in the $R\bar{3}m$ symmetry, clearly showing the stacked triangular planes of M, Ni, O.	8
3.1	Energy level diagrams for the configuration interaction calculations for NiO and MNiO_2 . Diagram based on those in [3, 4, 5]. The levels for a given n are broadened by the multiplet and crystal field terms, and mixed by the hopping terms.	13
4.1	Measured NiO XAS from [3], and calculated spectrum from this work. The features of the experimental spectrum are well reproduced in the calculated spectrum.	30
4.2	Calculated spectra for NiO for different values of U , illustrating the difficulty in using the spectrum to determine values for U	31
4.3	Calculated spectrum for NiO for varying values of $(pd\sigma)$. As in the previous figure, we see that the spectrum is insensitive to changes in parameters over a wide range.	32

4.4	Calculations for NaNiO_2 for the actual symmetry (via the Ewald sum of the terms in Eq. (3.12)) and for the approximate D_{4h} symmetry. The Ewald summation does not do a good job of reproducing the spectrum here, while the approximate symmetry can reproduce the actual symmetry calculation, as well as the experimental spectrum (see fig 4.6)	34
4.5	XAS for NaNiO_2 , with a e_g splitting from 0 to 1.6 eV. This splitting is much larger than that explained by the crystal field. This can be compared with the XAS for PrNiO_3 , the features of which look more like the undistorted spectrum.	35
4.6	Final calculated spectrum for NaNiO_2 , compared to experimental data from [3].	37
4.7	NaNiO_2 spectra for various values of Δ . Of particular interest is the movement of the shoulder peak of the 872 eV feature. . .	38
4.8	Calculated NaNiO_2 , with and without inclusion of the d^8 state, which raises the $3d$ occupation.	39
4.9	XAS data obtained via TEY and TFY measurements, for comparison to Fig. 4.11	40
4.10	XAS obtained by [3], [6]. These data, which are TEY data, are consistent with the TEY data obtained here, and hence different than the TFY data that is a more accurate probe of the bulk electronic structure.	41
4.11	Calculated and Experimental spectra for LiNiO_2 The qualitative features are reproduced, although less accurately than for NiO and NaNiO_2	42
4.12	Calculated spectrum for LiNiO_2 for the case of $10Dq = 0$, and for the case of a splitting of 0.7 eV on the Ni site and -0.6 eV on the ligand site.	43
4.13	LiNiO_2 vs. Δ . The movement of the feature between the two main peaks is what is of interest here. As expected, it is somewhat sensitive to Δ	44

4.14	LiNiO ₂ vs. $10Dq$. What is seen here is that the features of the 857 eV peak change as a function of $10Dq$, with a second shoulder peak at lower energy emerging as $10Dq$ is increased.	45
4.15	O K edge data from [4]. One can clearly see the feature opening up at 528-530 eV, below the conduction band spectrum, that is indicative of a hole on the O $2p$ orbital	47
4.16	O K edge data from this work. The feature at 530 eV observed in Fig. 4.15 is present in the TFY data, indicative of a hole on the O $2p$ shell.	48
4.17	Energy of the ground state as a function of Jahn-Teller distortion. The slope at 0 distortion is given, it is a factor of 10 larger for NaNiO ₂ than for LiNiO ₂	49
4.18	Diagram of NiO, NaNiO ₂ , and LiNiO ₂ , illustrating the effect of $\Delta < U$	50
4.19	Schematic of possibilities for the occupied O sites. The ground state will depend on the nature of the hole-hole nearest neighbour interaction on the O sites.	52
4.20	Schematic of couplings in a Ni ₂ O ₂ plaquette, mediated by two spin-1/2 holes on the O sites. The interaction J' is important here and its nature is unknown.	53
4.21	For a given ground state O hole occupation, there is the degeneracy of doublet formation between the spin on the Ni and the spin on the O	54

Chapter 1

Introduction and Description of Problem

1.1 Statement of the Jahn-Teller Problem

The materials NaNiO_2 and LiNiO_2 have been of interest to the condensed matter community for some time. LiNiO_2 is considered a candidate system for several exotic states, including frustrated quantum magnetism and resonating valence bonds. The central problem that has led to these suggestions is that, if one assumes that LiNiO_2 has a formal valency $\text{Li}^{1+}\text{Ni}^{3+}\text{O}_2^{2-}$, and further that the Ni is in the low spin configuration, then LiNiO_2 satisfies the criteria to undergo a Jahn-Teller distortion, wherein the degeneracy of the single unpaired electron is lifted by a crystal distortion and the formation of an orbitally ordered state. LiNiO_2 , however, does not undergo any observed ordering. Furthermore, NaNiO_2 does in fact undergo such a distortion, starting from the same crystal structure as LiNiO_2 . This unlifted degeneracy is what has given rise to the various suggestions of exotic states in LiNiO_2 , and is the motivation for the work done in this thesis.

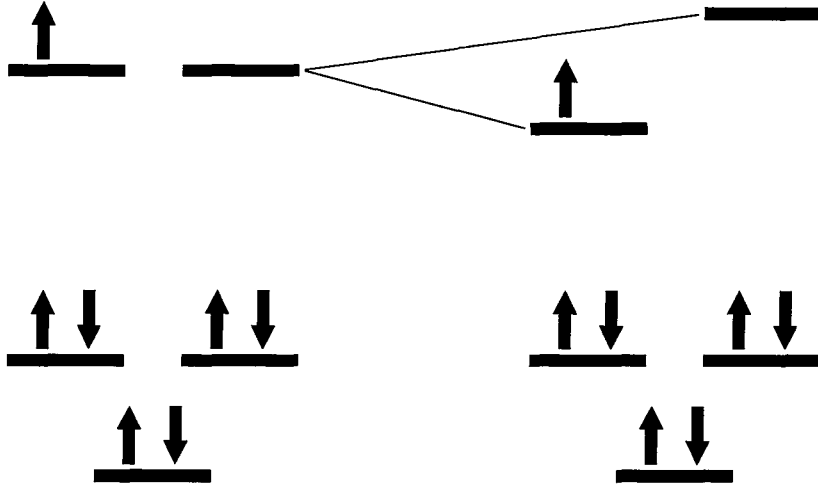


Figure 1.1: Schematic of the energy levels of the $3d$ Ni orbitals in NaNiO_2 . The crystal field splitting removes the lower three orbital, which are filled, leaving a single electron in a state degenerate in both spin and orbital degrees of freedom (left) which is broken below 480 K by the Jahn-Teller distortion (right).

1.2 Review of the Literature

Recent work in NaNiO_2 has determined conclusively its magnetic structure. ESR and magnetization work [1, 7] and inelastic neutron scattering [8] have formed a consistent picture of a triangular spin-1/2 lattice with FM spin-spin exchange in-plane and AFM exchange inter-plane. An orbital ordering accompanied by a Cooperative Jahn-Teller distortion occurs at 480 K, and a Neel ordering occurs at 23 K. This is consistent with the Hamiltonian derived by Mostovoy and Khomskii [9], which predicts that the orbital and spin degrees of freedom are decoupled. A schematic of the energy levels of the $3d$ Ni orbitals in NaNiO_2 is shown in Fig. 1.1. The lower levels are occupied and largely removed, leaving, in the high temperature case, a single electron degenerate in spin and orbit, degeneracies broken by the orbital ordering at 480 K and spin-orbit coupling.

The ground state of LiNiO_2 has been debated for some time now. An-

derson, in proposing the resonating valence bond, theorized that a triangular lattice anti-ferromagnet system would form a quantum liquid state[10], and LiNiO_2 has been proposed by Hirakawa as a candidate system for this to occur[11]. Whether or not LiNiO_2 actually forms a quantum liquid, though, depends crucially on the specific form of the magnetic interaction between Ni sites. Specifically, a ferromagnetic interaction leads to ferro-ordering, while an anti-ferromagnetic interaction leads to geometric frustration, and possibly formation of a resonating valence bond (RVB) state [10]. In the case of LiNiO_2 , the interactions of interest are the orbital interactions, as the orbital degree of freedom in a d shell with 7 electrons becomes a two-state system when the crystal field splitting is large enough to force the system into a low spin configuration. This has sparked interest in determining the magnetic interactions in LiNiO_2 . Hirakawa *et al.* [12] and Yoshizawa *et al.* [13] both reported featureless neutron data consistent with a lack of long range magnetic order, and anomalous behaviour in the magnetization, which Yoshizawa *et al.* attribute to the formation of a spin glass, as does Hirota *et al.* [14]. Reimers *et al.* [15], however, showed that there is a certain amount of exchange between Ni and Li sites, which occurs in all samples, regardless of stoichiometry. This site exchange can frustrate the ordering in LiNiO_2 , [16], if the in-plane and inter-plane spin magnetic interactions are the same as those found in NaNiO_2 [8], which has FM in-plane interactions and AFM inter-plane. Mostovoy and Khomskii, [9], and Holzapfel *et al.* [2] support this interpretation by pointing out that, in LiNiO_2 , the orbital and spin degrees of freedom decouple, implying that frustration of the magnetic ordering by spin-orbit interaction is unlikely.

Another approach, though, has found the lack of orbital order in LiNiO_2 to be intrinsic to the electronic structure of the compound. Kitaoka *et al.*, [17] attribute the lack of orbital order to quantum fluctuations melting a FM ordered state, based on NMR measurements. Reynaud *et al.* [18] propose a model with FM spin-spin interactions between electrons in the same orbital on two different sites, and AFM interactions between electrons on different orbitals, contradicting Mostovoy and Khomskii's calculation that the orbit and

spin are decoupled. Dare *et al.* [19] propose the crystal field splitting of the O $2p$ orbitals as a mechanism for introducing an AFM exchange path between Ni sites. Penc *et al.* [20] and Vernay *et al.* [21] use a spin-orbit model on a cluster in a mean field extrapolated out to large cluster size to conclude that the orbitally ordered state in NaNiO_2 and a spin-dimer quantum fluid state in LiNiO_2 can exist close enough in parameter space to explain the differences between NaNiO_2 and LiNiO_2 .

A third line of thinking has focussed on the hole-doped Mott insulator $\text{Li}_x\text{Ni}_{1-x}\text{O}$, using optical absorption measurements. Sawatzky and co-workers, [4, 5, 3] present a series of x-ray absorption spectroscopy (XAS), x-ray photoemission spectroscopy (XPS) and bremsstrahlung isochromat spectroscopy (BIS) measurements on the O $2p$ and Ni $3d$ electrons to establish that, in $\text{Li}_x\text{Ni}_{1-x}\text{O}$, the holes introduced by the Li go onto the O $2p$ orbitals, not the Ni $3d$ orbitals, leaving Ni with the valency $d^8\bar{L}$, where \bar{L} refers to a hole on the ligand orbital. Montoro *et al.* [6] and Kang *et al.* [22] have applied this to LiNiO_2 , however their data may not be accurate (see section 4.3), and they do not attempt to calculate the LiNiO_2 spectrum.

Broadly speaking, then, the literature on LiNiO_2 is divided into the following three categories: (1) intrinsic frustration of orbital ordering, either caused by competing FM and AFM exchange channels between Ni sites or quantum fluctuations arising from the degeneracy; (2) frustration caused by Ni ions in the Li layer, either as impurities or an exchange of Ni and Li sites; and (3) Ni $2+$ ions dominating due to O $2p$ hole occupancy, a possibility that most of the literature in the first two categories ignores. The explanation of why NaNiO_2 and LiNiO_2 , while isostructural, behave differently, is given, respectively, as: (1) the Jahn-Teller distortion is sensitive to small changes in parameters arising from crystal structure; (2) Li is closer in size to Ni than Na is, thus making exchange of Li and Ni more likely; (3) the different crystal environment changes the electronegativity of the O ions, thus making the Ni^{2+} state more likely in LiNiO_2 . This thesis applies a sophisticated configuration interaction (CI) routine, XTLS 8.30 [23], to new XAS data on LiNiO_2 , to determine the

formal valency of Ni in this compound. We also examine NaNiO_2 and NiO for comparison.

Chapter 2

Description of Materials and Measurement

2.1 Crystal Structure

The NiO crystal forms a NaCl structure, with alternating Ni and O sites[24]. The formal valency in this situation is Ni^{2+} , O^{2-} . In the materials LiNiO_2 and NaNiO_2 , above 480 K, every other layer of Ni ions is replaced by a layer of Li or Na ions, respectively, distorting the crystal structure and removing the fourfold rotation symmetries of the cubic symmetry, leaving a three-fold rotation and the point group D_{3d} in the space group $R\bar{3}m$, as visualized in Fig. 2.1[25]. The symmetry operations in this case are a three-fold rotation axis down the c-axis, three two-fold rotation axis perpendicular to the c-axis, and inversion (which generates a series of mirror planes). In NaNiO_2 , there is a further lowering of symmetry due to a cooperative Jahn-Teller distortion at 480K, to a C_{2h} point group with a $C2/m$ space group, which removes all orbital degeneracy [1, 7]. This transition elongates the O octehedra surrounding the Ni ion along one axis. Thus the nearest neighbour Ni-O bonds go from six of equal length (1.98 Å) to four shorter (1.91 Å) and two longer (2.14 Å) bonds[1].

The $R\bar{3}m$ phase can be viewed as a four-atom unit cell, with the following

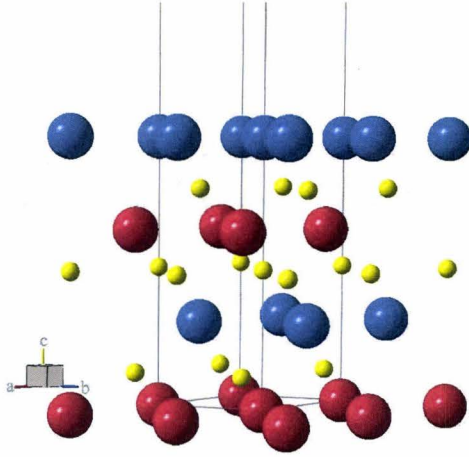


Figure 2.1: Crystal structure of MnO_2 , in the $R\bar{3}m$ symmetry, clearly showing the stacked triangular planes of M, Ni, O.

primitive translation vectors:

$$\begin{aligned}\mathbf{a}_1 &= (a\sqrt{3}/6, a/2, c/3) \\ \mathbf{a}_2 &= (a\sqrt{3}/6, -a/2, c/3) \\ \mathbf{a}_3 &= (-2a\sqrt{3}/6, 0, c/3)\end{aligned}$$

In the same coordinate system, the other three ions not at the origin are all on the z (c) axis:

$$\begin{aligned}\tau_{\text{Ni}} &= (0, 0, 0) \\ \tau_{\text{M}} &= (0, 0, c/2) \\ \tau_{\text{O1}} &= (0, 0, x(O)c) \\ \tau_{\text{O2}} &= (0, 0, (1 - x(O))c)\end{aligned}$$

It is often useful to approximate a lower symmetry by a higher one, which simplifies the crystal field and hopping terms that will be discussed later. However one should ask what the effect will be of making this approximation.

Material	$a(\text{\AA})$	$b(\text{\AA})$	$c(\text{\AA})$	β	$x(O)$	$z(O)$
NaNiO ₂	5.31	2.84	5.57	110.44	0.282	0.799
LiNiO ₂	4.98	2.87	5.01	109.3	0.26	0.77

Table 2.1: Room temperature crystal parameters. The NaNiO₂ parameters were taken from [1], while LiNiO₂ was taken from [2]. Both are given in terms of the $C2/m$ structure.

For the purposes of this thesis, the approximation we want to consider is modeling the transition $D_{3d} \rightarrow C_2$ as the transition $O_h \rightarrow D_{4h}$. Physically, this can be pictured as assuming that the six surrounding O ions around a given Ni ion are in a regular octehedral arrangement, instead of the distorted one which is the real case, and then viewing the Jahn-Teller distotion as an elongation of the octehedra along one axis. Since in both the $D_{3d} \rightarrow C_2$ and $O_h \rightarrow D_{4h}$ cases, the O ions go from six equidistant ions to a set of four equidistant ions and a set of two equidistant ions, what we want to look at is how the bond angle changes. From [2], we have the following bond angles: for LiNiO₂, there are 6 angles of 93.2, and a corresponding six at 86.6, while for NaNiO₂, there four at 94.8, and two at 95.1, again with their complimentary angles. The difference between this and the octehedral case, is a 0.003 Å difference in the position of the nearest neighbour O ions. We will discuss the effects that this approximation has in the sections on the relevant terms below.

2.2 Materials Synthesis and Measurement

The data for NaNiO₂ and NiO was taken from [3]. The LiNiO₂ samples measured were provided by the neutron scattering group of Bruce Gaulin at McMaster.

The data analysed in this thesis is x-ray absorption spectra (XAS) of LiNiO₂, NaNiO₂, and NiO. The absorption processes we look at are the Ni L edge and the O K edge. The Ni L edge consists of an absorption process that excites a $2p$ core electron on the Ni ion to the $3d$ valence shell, $2p^6 3d^n \rightarrow 2p^5 3d^{n+1}$. This process is expected to occur in the energy range

835-850 eV. Two broad peaks are expected, due to the large core spin-orbit coupling, with finer details present in each that depend on the available $3d$ states [3]. The O K edge consists of an absorption process that excites a $1s$ electron on the O ion into a valence state just above the $2p$ levels. In both cases what is measured are the decay products of the core hole, either Auger electrons (TEY) or emitted photons (TFY).

The Ni L edge and O K edge measurements were performed at the SGM beamline of the Canadian Light Source. The sample was at room temperature, in a vacuum with a pressure of 5×10^{-9} mbar. The TFY measurements require a self-absorption correction, which was done following [26], using the data tabulated in [27].

The samples of LiNiO_2 used in this thesis were measured with both total electron yield (TEY) and total fluorescence yield (TFY). Measurements taken from [3, 6] used TEY measurements and, to our knowledge, did not perform TFY measurements for comparison. The TEY technique measures all electrons escaping the sample for a given incident photon energy. It is assumed that the majority of the electrons emitted are Auger electrons coming from the decay of the $2p$ hole created by the incident photon. Whether this assumption is valid is the source of ongoing controversy, but the ease of measurement makes this a widely used technique in XAS. For our purposes, more relevant is the probing depth of the procedure. The depth is limited to the mean free path of the emitted electrons in the substance studied, which, for NiO, NaNiO_2 , and LiNiO_2 , is ~ 20 Angstroms [28]. For NiO and NaNiO_2 , both of which can be made in high quality, this is probably not a significant limitation. For LiNiO_2 , however, the tendency of Li_2O to precipitate out of the sample and collect on the surface, which, for a powder sample, cannot be adequately cleaned, makes a probe of the bulk sample desirable. TFY is limited only by the mean free path of the x-rays emitted, which is large enough to ensure probing of the bulk sample.

Chapter 3

Theory of Configuration Interaction

3.1 The Hamiltonian

In analysing the XAS data, we use a configuration interaction (CI) Hamiltonian, which considers, in the initial state, the $3d$ orbitals of a single Ni ion. Electrons occupying the ten states in the $3d$ orbital sit in an external potential created by the crystal field, and interact with each other via the Coulomb interaction. To take into account the surrounding ligand orbitals (the O $2p$ band), we introduce a hopping term between the Ni site and the ligand band, which we consider to be at some energy Δ relative to the Ni orbitals. In the excited state, we consider the Ni $2p$ core electrons; both the spin-orbit coupling in those states, and the Coulomb interaction between the $2p$ electrons and the $3d$ electrons.

Thus we have the following [3]:

$$H = H_0 + H_U + H_{so} \tag{3.1}$$

where

$$H_0 = \sum_{\mu} \epsilon_d(\mu, \mu') d_{\mu}^{\dagger} d_{\mu'} + \sum_{\nu, i} \epsilon_p(\nu, \nu') p_{\nu, i}^{\dagger} p_{\nu', i} + \sum_{\mu, \nu} [t_{pd}(\mu, \nu) d_{\mu}^{\dagger} p_{\nu} + H.c.] \quad (3.2)$$

$$H_U = \sum_{\mu_1, \mu_2, \mu_3, \mu_4} U_{dd}(\mu_1, \mu_2, \mu_3, \mu_4) d_{\mu_1}^{\dagger} d_{\mu_2} d_{\mu_3}^{\dagger} d_{\mu_4} \quad (3.3)$$

$$H_{so} = \sum_{\gamma, \gamma'} \zeta_p \langle \gamma | \mathbf{l} \cdot \mathbf{s} | \gamma' \rangle c_{\gamma}^{\dagger} c_{\gamma'} + \sum_{\mu, \gamma, \mu', \gamma'} U_{pd}(\mu, \gamma, \mu', \gamma') d_{\mu}^{\dagger} d_{\mu'} c_{\gamma}^{\dagger} c_{\gamma'} \quad (3.4)$$

where μ indexes orbit and spin of the Ni d-orbitals and ν indexes the O p-orbitals. We want to work out the matrix elements in the configuration interaction scheme of a cluster consisting of a Ni ion and a surrounding oxygen octahedron, which we will account for as a ligand orbital. To do so, we use the following basis:

$$\begin{aligned} |d_{\mu, \mu', \mu''}^7\rangle_i &= d_{\mu} d_{\mu'} d_{\mu''} |d^{10}\rangle |p^{10}\rangle \\ |d_{\mu, \mu'}^8 \underline{L}_{\nu}\rangle_i &= d_{\mu} d_{\mu'} p_{\nu} |d^{10}\rangle |p^{10}\rangle \\ |d_{\mu}^9 \underline{L}_{\nu, \nu'}^2\rangle_i &= d_{\mu} p_{\nu} p_{\nu'} |d^{10}\rangle |p^{10}\rangle \\ |d^{10} \underline{L}_{\nu, \nu', \nu''}^3\rangle_i &= p_{\nu} p_{\nu'} p_{\nu''} |d^{10}\rangle |p^{10}\rangle \end{aligned} \quad (3.5)$$

for the initial state, and, for the final state, with a 2p electron excited into the 3d shell,

$$\begin{aligned} |d_{\mu, \mu'}^8\rangle_{f, \gamma} &= d_{\mu} d_{\mu'} c_{\gamma} |d^{10}\rangle |p^{10}\rangle |p^6\rangle \\ |d_{\mu}^9 \underline{L}_{\nu}\rangle_{f, \gamma} &= d_{\mu} p_{\nu} c_{\gamma} |d^{10}\rangle |p^{10}\rangle |p^6\rangle \\ |d^{10} \underline{L}_{\nu, \nu'}^2\rangle_{f, \gamma} &= p_{\nu} p_{\nu'} c_{\gamma} |d^{10}\rangle |p^{10}\rangle |p^6\rangle \end{aligned} \quad (3.6)$$

where $|p^{10}\rangle$ refers to the ligand p orbitals, and $|p^6\rangle$ refers to the Ni core 2p orbital. Here the combination of ligand O 2p orbitals is taken to be a d

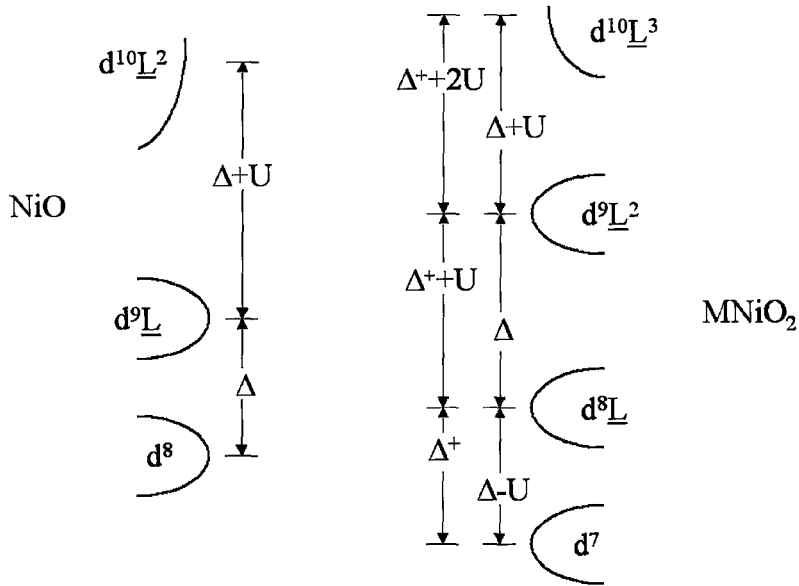


Figure 3.1: Energy level diagrams for the configuration interaction calculations for NiO and MNiO₂. Diagram based on those in [3, 4, 5]. The levels for a given n are broadened by the multiplet and crystal field terms, and mixed by the hopping terms.

orbital labelled as $|p^{10}\rangle$; this approximation is equivalent to *a priori* taking into account the selection rules governing hopping from the O $2p$ band to the Ni $3d$ orbital.

3.2 The single particle matrix elements

First we consider the matrix elements of 3.2: $\epsilon_{d,p}$ and t_{pd} . $\epsilon_{d,p}$ will be determined by the crystal field splitting, and Δ , the charge-transfer energy. The t_{pd} terms will consist of Slater-Koster integrals. We will consider each of these.

3.2.1 The crystal field

For the potential at the origin due to the crystal ions, we have

$$V(\vec{r}) \propto \sum_{\vec{R}} \frac{1}{|\vec{r} - \vec{R}|}$$

To find the matrix of the Hamiltonian in the single particle basis, we use the following identity:

$$\frac{1}{|\vec{r} - \vec{R}|} = \sum_{l=0}^{\infty} \sum_{m=-l}^l \frac{r^l}{R^{l+1}} \frac{4\pi}{2l+1} Y_{l,m}^*(\Theta, \Phi) Y_{l,m}(\theta, \phi) \quad (3.7)$$

where $\vec{R} = (R, \Theta, \Phi)$, $Y_{l,m}$ is the usual spherical harmonics, and where we have assumed that $R > r$, to get

$$V(\vec{r}) = Ze^2 \sum_{\vec{R}} \sum_{l=0}^{\infty} \sum_{m=-l}^l \frac{r^l}{R^{l+1}} \frac{4\pi}{2l+1} Y_{l,m}^*(\Theta, \Phi) Y_{l,m}(\theta, \phi) \quad (3.8)$$

In this form, we can cast the problem in terms of perturbation theory, with

$$H = H_{atom} + V$$

where H_{atom} is the hamiltonian of the atom in free space, for which we want to consider the degenerate $3d$ orbitals, which will have the form

$$|\psi_m\rangle = f(r)Y_{2,m}$$

where $f(r)$ is the radial dependence.

Thus, to use first order degenerate perturbation theory, we consider the

integral:

$$\begin{aligned} \langle \psi_{m'} | V | \psi_{m''} \rangle &= Z e^2 \sum_{l=0}^{\infty} \sum_{m=-l}^l \left(\sum_{\vec{R}} 4\pi \frac{Y_{l,m}^*(\Theta, \Phi)}{R^{l+1}} \right) \frac{1}{2l+1} \langle r^l \rangle (-1)^{m'} \\ &\times \int Y_{2,-m'} Y_{l,m} Y_{2,m''} \sin \theta d\theta d\phi \end{aligned} \quad (3.9)$$

We know that

$$\begin{aligned} \int Y_{2,-m'} Y_{l,m} Y_{2,m''} \sin \theta d\theta d\phi &= \sqrt{\frac{(4+1)(2l+1)(4+1)}{4\pi}} \\ &\times \begin{pmatrix} 2 & l & 2 \\ 0 & 0 & 0 \end{pmatrix} \begin{pmatrix} 2 & l & 2 \\ -m' & m & m'' \end{pmatrix} \end{aligned} \quad (3.10)$$

Where

$$\begin{pmatrix} l_1 & l_2 & l_3 \\ m_1 & m_2 & m_3 \end{pmatrix}$$

are the Wigner 3j symbols [29]. From the properties of the Wigner 3j symbols[29], namely,

$$|l_1| + |l_2| \geq |l_3|$$

we can see that

$$|2-l| \leq 2 \leq 2+l$$

$$0 \leq l \leq 4$$

Also, since

$$\begin{pmatrix} 2 & l & 2 \\ 0 & 0 & 0 \end{pmatrix} = 0$$

for $2+l+2$ odd, then l must be even. So $l = 0, 2, 4$ are the only non-zero terms. In addition, we have the condition that

$$m_1 + m_2 + m_3 = 0$$

So that, for a given m , the only non-zero terms are those matrix elements for

which

$$m' + m'' = m$$

So, defining

$$5\sqrt{\frac{4\pi}{2l+1}} \begin{pmatrix} 2 & l & 2 \\ 0 & 0 & 0 \end{pmatrix} \begin{pmatrix} 2 & l & 2 \\ -m' & m & m'' \end{pmatrix} \equiv w_{l,m',m,m''}$$

we have

$$\langle \psi_{m'} | V | \psi_{m''} \rangle = \sum_{\substack{l=0,2,4 \\ l \geq m'+m''}} \left(\sum_{\bar{R}} \frac{Y_{l,m'+m''}^*(\Theta, \Phi)}{R^{l+1}} \right) (-1)^{m'} \langle r^l \rangle w_{l,m',m'+m'',m''} \quad (3.11)$$

Since the values of the various Wigner 3-j symbols are known, we are left with two things we need to calculate: the radial moments of the wavefunctions, and the term

$$\sum_{\bar{R}} \frac{Y_{l,m}^*}{R^{l+1}} \quad (3.12)$$

from Eq. (3.11), for $l = 0, 2, 4$.

There are two approaches we will consider for this thesis. In the first, we use tabulated values for the many electron atomic wavefunctions in the Hartree-Fock approach [30] to estimate the radial integrals, and use the Ewald summation (see appendix A) to calculate the terms Eq. (3.12) over the infinite crystal. The consensus in the literature [31] is that this method will give the ordering of the eigenstates and a rough guess as to the magnitude of the splitting, in cases where the splitting is well defined. The second approach, which will be taken up in the next section in more detail, is to use the apparatus of group theory to reduce the crystal field terms to one or two parameters based on the (approximate) symmetry of the crystal that can be varied to determine an empirical best fit to some measured spectrum.

3.2.2 Group Theory and the symmetry specific form for the crystal field

To put the crystal field into a form that explicitly takes into account the symmetry of the lattice, we make use of group theory. Specifically, if R , some rotation and/or reflection operator, commutes with H , the Hamiltonian, then there are no matrix elements of H between states which are eigenstates of R with different eigenvalues of R [32]. Thus, classifying our orbital wavefunctions in terms of their properties under symmetry operations of the lattice, which commute with the crystal field Hamiltonian, will greatly simplify the Hamiltonian by allowing us to set many of the matrix elements to zero. To make use of this analysis, we will work in a basis that makes the angular dependence on x, y, z explicit:

$$Y_{2,0} = \frac{1}{4} \sqrt{\frac{5}{\pi}} \left(\frac{3z^2}{r^2} - 1 \right) = \langle \theta, \phi | 3z^2 - r^2 \rangle \quad (3.13)$$

$$\frac{-1}{\sqrt{2}} (Y_{2,1} - Y_{2,-1}) = \frac{-1}{4} \sqrt{\frac{15}{\pi}} \left(\frac{xz}{r^2} \right) = \langle \theta, \phi | xz \rangle \quad (3.14)$$

$$\frac{i}{\sqrt{2}} (Y_{2,1} + Y_{2,-1}) = \frac{1}{4} \sqrt{\frac{15}{\pi}} \frac{yz}{r^2} = \langle \theta, \phi | yz \rangle \quad (3.15)$$

$$\frac{1}{\sqrt{2}} (Y_{2,2} + Y_{2,-2}) = \frac{1}{8} \sqrt{\frac{15}{\pi}} \frac{x^2 - y^2}{r^2} = \langle \theta, \phi | x^2 - y^2 \rangle \quad (3.16)$$

$$\frac{i}{\sqrt{2}} (Y_{2,-2} - Y_{2,2}) = \frac{1}{8} \sqrt{\frac{15}{\pi}} \frac{xy}{r^2} = \langle \theta, \phi | xy \rangle \quad (3.17)$$

We can now examine which group representations each of these forms transforms under, which have been tabulated for convenience [32].

Under the O_h group, character tables in [32] show that the quadratic forms $(3z^2 - r^2, x^2 - y^2)$ transform into each other under the E representation, while the forms (xy, xz, yz) transform into each other under the T_2 representation. One way of visualizing this physically is to consider the permutation of the coordinate axes, which leaves the Hamiltonian invariant for the O_h case. Sending $x \rightarrow y, y \rightarrow z, z \rightarrow x$ obviously sends the set (xy, xz, yz) onto itself, and,

also, under this permutation, it can be seen that the set $(3z^2 - r^2, x^2 - y^2)$ also transforms onto itself.

Following standard notation, the eigenstates (3.13) and (3.16) are referred to as the e_g orbitals (transforming like E), and the states 3.14, 3.15, and 3.17 are the t_{2g} orbitals (transforming under T_2). While symmetry considerations determine only the degeneracies, and not the actual energy levels of these states, general physical arguments show that, for an atom surrounded by an octahedron of negatively charged atoms, the e_g level will be at a higher energy than the t_{2g} level. So for this case there are two energy levels, and applying the condition that the energies add to 0 reduces this to one splitting parameter, traditionally referred to as $10Dq$. The condition that the energy sums to zero is simply the condition that it is the $l = 2, 4$ sums in Eq. (3.12) that are of consequence, as the $l = 0$ sum will be taken into account in Δ .

For the symmetry D_{4h} , the fact that the reflection planes in the xy, xz , and yz planes remain implies that the eigenstates of O_h remain, but the degeneracies have been removed (as permutation of axes no longer commutes with the Hamiltonian), except for the degeneracy of the $|xz\rangle, |yz\rangle$ states that arises from the remaining four-fold rotation axis. This leaves three parameters, as there are four energy states and the condition that the energies add up to zero.

For D_{3d} , the situation is more complicated. The character table implies that, in distorting from O_h to D_{3d} , there will still be two states transforming under the E representation, while the T_2 representation will be split into E and A_1 ; thus there will be three energy levels. There will also be a free parameter that determines the eigenstates of the system, which will be dependent on the choice of coordinates. Of course, the eigenstates of O_h are also dependant on the choice of coordinates, but in that case there is an obvious and widely used choice, which is not the case for D_{3d} . In this work the D_{3d} symmetry will be taken into account via the Madelung sum over an infinite crystal in a point-charge approximation; the general form will not be used.

For the C_{2h} symmetry, very little can be determined from group theoretical calculations, on account of the low number of symmetry transformations

(namely, one two-fold rotation and one mirror plane). There are no degeneracies in the general case. However as C_{2h} is contained in D_{3d} , D_{4h} , and O_h , certain parameters for a crystal with a C_{2h} point group will lead to the situations discussed above.

3.2.3 The Hopping terms

H_t describes the hopping from one ion to another. Here, we restrict hopping to O-Ni hopping. The hopping elements will be the overlap of the wavefunction on one site with the wavefunction on another; that is, we want the integral

$$t_{pd}(\mu, \nu) = \int \psi_\mu^\dagger(\mathbf{r}) H \psi_\nu(\mathbf{r} - \mathbf{R}_i) d\mathbf{r} \quad (3.18)$$

where H in 3.18 represents the kinetic and external potential energy operators. We simplify this integral by making the approximations that the wavefunctions involved are atomic orbitals, and furthermore, that the only potential we consider is the potential due to the ions at the origin and at the site \mathbf{R}_i ; *i.e.*, we neglect the crystal field. Doing this allows us to take the vector \mathbf{R}_i as our \mathbf{e}_z vector and quantize the angular momentum around it. The standard notation for this is to label the orbital angular momentum eigenstates with respect to the axis joining the atomic centres as, for the p orbital, $p\sigma$ and $p\pi_\pm$ for $m_l = 0$ and $m_l = \pm 1$, respectively, and for the d orbital, $d\sigma$, $d\pi_\pm$, and $d\delta_\pm$, for $m_l = 0$, $m_l = \pm 1$, and $m_l = \pm 2$, respectively. Once so labeled, we can note that, as the two centre approximation has rotational symmetry about the inter-atomic axis, l along that axis is a good quantum number, and thus there will be no mixing of orbitals with different m_l values. So, we can label the integrals like Eq. (3.18) with $m_l = 0$ as $(pd\sigma)$, and the components with $m_l = \pm 1$ as $(pd\pi)$ (for hopping from a d orbital to a p orbital), and leave these integrals, which will in general be difficult, to be fitted empirically. Then, the only remaining task is to determine the coefficients for these integrals for some general hopping from a d orbital at the origin to a p orbital at an arbitrary direction. These coefficients have been tabulated in terms of direction cosines [33]. The result

of most interest to this thesis is that for the case in which the surrounding ions form a regular octahedra, for which we can take each of the ions to lie on one of the x, y, z axes. Considering the ions that lie on the z axis, our usual spherical harmonics are already quantized with respect to the axis between the atoms. To use this we need, in addition to Eq. (3.13-3.17) for the d orbitals, the following for the p orbitals:

$$Y_{1,0} = \frac{1}{2} \sqrt{\frac{5}{\pi}} \left(\frac{z}{r} \right) = \langle \theta, \phi | z \rangle \quad (3.19)$$

$$\frac{1}{\sqrt{2}} (Y_{1,1} - Y_{1,-1}) = -\frac{1}{4} \sqrt{\frac{3}{\pi}} \left(\frac{x}{r} \right) = \langle \theta, \phi | x \rangle \quad (3.20)$$

$$\frac{i}{\sqrt{2}} (Y_{1,1} + Y_{1,-1}) = \frac{1}{4} \sqrt{\frac{3}{\pi}} \left(\frac{y}{r} \right) = \langle \theta, \phi | y \rangle \quad (3.21)$$

So, upon inspection, we can see that the only two orbitals with $m_l = 0$ are $|3z^2 - r^2\rangle$ and $|z\rangle$. Thus the only overlap involving the integral $(pd\sigma)$ is $E_{3z^2-r^2,z} = (pd\sigma)$ (using Slater's notation [33]). Also, the orbitals $|xy\rangle$ and $|x^2 - y^2\rangle$ are composed of $|m_l| = 2$ harmonics, and thus will not have any overlap with the p orbitals. Also, we can see that, if we assume that $(pd\pi)_- = (pd\pi)_+ = (pd\pi)$, then the matrix elements between orbitals like $Y_1 + Y_{-1}$ and $Y_1 - Y_{-1}$ will be zero, which leaves, as the only non-zero elements,

$$E_{yz,y} = E_{xz,x} = (pd\pi)$$

We could now consider the general rotation from this case, but it will suffice to consider permutations of the axes. Note that all permutations of x, y, z will take t_{2g} orbitals onto other t_{2g} orbitals, and e_g orbitals onto other e_g orbitals. Thus in the octahedral case, only e_g orbitals participate in σ bonding, while only t_{2g} orbitals participate in π bonding.

For the t_{2g} orbitals, the permutations leave, for an atom on the x axis, the non-zero elements are:

$$E_{xz,z} = E_{xy,y} = (pd\pi)$$

and, for an atom on the y axis,

$$E_{xy,x} = E_{yz,z} = (pd\pi)$$

For the e_g orbitals, we need the following:

$$|y^2 - z^2\rangle = - \left(\frac{\sqrt{3}}{2} |3z^2 - r^2\rangle + |x^2 - y^2\rangle \right) \quad (3.22)$$

$$|z^2 - x^2\rangle = \left(\frac{\sqrt{3}}{2} |3z^2 - r^2\rangle - |x^2 - y^2\rangle \right) \quad (3.23)$$

from which we can conclude that terms we want are:

$$E_{x^2-y^2,x} = \frac{-\sqrt{3}}{2} (pd\sigma) \quad (3.24)$$

$$E_{x^2-y^2,y} = \frac{\sqrt{3}}{2} (pd\sigma) \quad (3.25)$$

Thus, adding the contributions from the ions on the positive and negative axis, for the case with cubic symmetry, we can take our hopping elements to be[33]:

$$t_{pd}(3z^2 - r^2) = \sqrt{3}(pd\sigma) \quad (3.26)$$

$$t_{pd}(x^2 - y^2) = \sqrt{3}(pd\sigma) \quad (3.27)$$

$$t_{pd}(xy) = 2(pd\pi) \quad (3.28)$$

$$t_{pd}(xz) = 2(pd\pi) \quad (3.29)$$

$$t_{pd}(yz) = 2(pd\pi) \quad (3.30)$$

3.3 The two particle matrix elements

Since we have more than one hole on the Ni d orbitals, we must consider the terms in our Hamiltonian that correspond to interaction terms between different configurations of putting three holes on the ten possible sites on the d-orbital. We consider only the electrostatic interaction between electrons. The derivation that follows will roughly follow [34], with notations updated for

consistency. Disregarding the magnetic interaction leaves both orbital angular momentum and spin angular momentum as good quantum numbers for the central field problem, so we can diagonalize the multiplet Hamiltonian by choosing angular momentum eigenstates. To enumerate then the states, we simply have to count the number of combinations of states with M_L and M_S allowed by the number of electrons present and the angular momentum states that they are in. So, considering the state with one electron, or equivalently, one hole, in the d-orbital, the state must be a spin-1/2, $l = 2$ state. For two or electrons or holes, we can have singlet states (spin-0) or triplet states (spin-1). Considering the possible combinations of orbital occupations, the singlet states will have angular momenta given by $l = 0$, $l = 2$, or $l = 4$, while the triplet state allows $l = 1$ or $l = 3$. Less obvious is the possible states given by three electrons or holes: for the doublet ($S = 1/2$), $l = 1$, $l = 2$ (two different ways) $l = 3$, and $l = 4$, while for the quadruplet ($S = 3/2$), $l = 1$ and $l = 3$ [34]. Starting from this point, we can use wave mechanics to reduce the interaction integrals between the various wavefunctions that make up these eigenstates.

The two electron term, e^2/r_{ij} , is non-trivial for multiple electron (hole) states. In wave notation, we have:

$$\langle \psi_i \psi_j | \frac{e^2}{r_{12}} | \psi_r \psi_t \rangle = \int_1 \int_2 \psi_i^\dagger(\mathbf{r}_1) \psi_i^\dagger(\mathbf{r}_2) \frac{e^2}{r_{12}} \psi_r(\mathbf{r}_1) \psi_t(\mathbf{r}_2) \quad (3.31)$$

To do this integral we expand the potential by means of the identity used previously:

$$\frac{1}{|\mathbf{r}_i - \mathbf{r}_j|} = \sum_{l=0}^{\infty} \sum_{m=-l}^l \frac{4\pi}{2l+1} \frac{r_{<}}{r_{>}} \overline{Y}_{l_1}^{m_1} Y_{l_2}^{m_2} \quad (3.32)$$

where $r_{<}$ and $r_{>}$ are the lesser and greater of r_i and r_j . Since our wavefunctions are atomic orbitals, the angular components will be given by spherical harmonics, so the properties used in section 3.2.1 will apply here as well. Doing so, and recalling the properties of the Wigner 3j symbols, allows us to reduce Eq. (3.31) to the form:

$$\begin{aligned} \langle ij | \frac{e^2}{r_{12}} | rt \rangle &= \delta_{m_{si}, m_{sr}} \delta_{m_{sj}, m_{st}} \delta_{m_{li} + m_{lj}, m_{lr} + m_{lt}} \\ &\times \sum_{k=0}^{\infty} c^k(l_i m_i; l_r m_r) c^k(l_t m_t; l_j m_j) R^k(ij; rt) \end{aligned} \quad (3.33)$$

where we define

$$\begin{aligned} c^k(l_i m_i; l_r m_r) &= \sqrt{\frac{4\pi}{2l+1}} \int Y_{l_i}^{|m_i|} Y_{l_r}^{|m_r|} Y_k^{m_i - m_r} d\Omega \\ &\times (-1)^{(m_i + |m_i| + m_r + |m_r| + (m_i - m_r) + |m_i - m_r|)/2} \end{aligned} \quad (3.34)$$

and

$$\begin{aligned} R^k(ij; rt) &= \int_0^{\infty} \int_0^{\infty} R_{n_i l_i}^{\dagger}(r_1) R_{n_j l_j}^{\dagger}(r_2) R_{n_r l_r}(r_1) R_{n_t l_t}(r_2) \\ &\times \frac{r_{\leq}^k}{r_{>}^{k+1}} r_1^2 r_2^2 dr_1 dr_2 \end{aligned} \quad (3.35)$$

where $R(r)$ and $Y_l^m(\theta, \phi)$ are the usual radial and angular components of the wavefunction. Now, since we label our states by angular momentum, in which basis the electron-electron Hamiltonian is diagonal, we will be considering matrix elements that look like:

$$\langle ij | H | ij \rangle$$

while, for the terms between the d electrons and those in the core p orbitals, which we will want to consider for the XAS comparison, we will have terms of the form

$$\langle ij | H | ij \rangle \pm \langle ij | H | ji \rangle$$

i.e., the direct energy and the exchange energy. So, we can define the following

l	m	$F^2(dd)$	$F^4(dd)$
3	1	-58/441	5/441
1	1	77/441	-70/441
4	0	50/441	15/441
2	0	-13/441	50/441
0	0	140/441	140/441

Table 3.1: Diagonal matrix elements for d^2 .

l	m	$F^2(dd)$	$F^4(dd)$
3	3/2	-93/441	-30/441
2	3/2	42/441	-105/441
5	1/2	-12/441	30/441
4	1/2	-57/441	55/441
3	1/2	123/441	-45/441
2	1/2	105/441	105/441
2	1/2	69/441	-15/441
1	1/2	-12/441	30/441

Table 3.2: Diagonal matrix elements for d^3 .

Slater integrals:

$$F^k(n_i l_i; n_j l_j) = R^k(ij; ij) \quad (3.36)$$

$$G^{jk}(n_i l_i; n_j l_j) = R^k(ij; ji) \quad (3.37)$$

so that

$$\langle ij | \frac{e^2}{r_{12}} | ij \rangle = \sum_{k=0}^{\infty} c^k(l_i m_i; l_i m_i) c^k(l_j m_j; l_j m_j) F^k(n_i l_i; n_j l_j) \quad (3.38)$$

$$\langle ij | \frac{e^2}{r_{12}} | ji \rangle = \delta_{m_{si}, m_{sj}} \sum_{k=0}^{\infty} [c^k(l_i m_i; l_j m_j)]^2 G^{jk}(n_i l_i; n_j l_j) \quad (3.39)$$

Now, as we saw in section 3.2.1, the angular integrals are known (since the angular wavefunctions are), while the radial integrals are, in general, not. The angular integrals are sums of Wigner $3j$ coefficients, which are tabulated in [34], and listed here in Tables 3.1 and 3.2.

The parameter U is the energy difference of the lowest energy state of

one multiplet to the next[35]; ie, instead of including $F^0(dd)$, explicitly, we determine it implicitly as being the value that makes the lowest energy of some multiplet state we choose, as in Fig. 3.1.

A commonly used convention in multiplet calculation is the Racah parameters. These are given by:

$$A = A_0 - \frac{49}{441}F^4(dd) \quad (3.40)$$

$$B = \frac{1}{49}F^2(dd) - \frac{5}{441}F^4(dd) \quad (3.41)$$

$$C = \frac{35}{441}F^4(dd) \quad (3.42)$$

where A_0 is a multiple of F^0 , and hence determined by U_{dd} . These parameters have, in addition to the removal of some unwieldy coefficients in Table 3.2, the property that the ratio B/C is expected to be largely independent of the radial distribution, and hence the specific material.

3.4 Calculating the Spectra

Enumerating the possible occupations of 2-3 holes on the 10 $3d$ orbital states and the corresponding 10 ligand states produces an enormous number (~ 10000) of basis states. To take these into account, some groups have simplified the states; *e.g.*, [36] takes into account only whether the orbital is e_g or t_{2g} , not which orbital it is. In this work, the calculation uses the full basis, with a Lanczos-type large matrix diagonalization routine (referred to as the Haydock Recursion method) to obtain the lowest energies and eigenstates [28]. This requires using the theory outlined above to calculate $H|\psi\rangle$ for a given state vector $|\psi\rangle$. The Lanczos algorithm repeatedly applies H to a randomized vector to generate a subspace of n basis vectors, where n is much less than the original number of basis states, and where, for increasing n , the procedure produces the ground state with arbitrary accuracy. While this has the benefit of presumably being more accurate, as it considers all states as unique, as

well as allowing crystal field symmetries lower than those possible in [36], the drawback is that one cannot confine the calculation to a specific angular momentum manifold without determining *a priori* what basis states belong to that manifold.

The configuration interaction calculation provides initial and final states and energies for the process of absorption of an x-ray with the excitation $2p^63d^n \rightarrow 2p^53d^{n+1}$, referred to as the Ni L edge. The difference in energy between the initial and final states will determine the energies of the possible transitions, while the amplitude of the transitions will be determined by the transition matrix; that is, we will have the following spectral function [23]:

$$F(\omega) = \sum_f |\langle f|T(\omega)|i\rangle|^2 \delta(\omega + E_i - E_f) \quad (3.43)$$

where ω is the energy of the absorbed photon, $T(\omega)$ the transition matrix. For XAS, we can take the transition matrix to simply be the dipole operator. So:

$$T(\omega) = T = \sum_i \mathbf{r}_i \quad (3.44)$$

Since the dipole operator is a sum of single particle operators, then we need only consider the matrix elements $\langle \psi_k(\mathbf{r})|\mathbf{r}|\psi_{k'}(\mathbf{r})\rangle$. The transitions we are considering are those from the $2p$ shell to the $3d$ shell, which means that we want elements of the form $\langle \psi_{1,1,m_l,m_s}(\mathbf{r})|\mathbf{r}|\psi_{2,2,m_l,m_s}(\mathbf{r})\rangle$.

These elements can be greatly simplified by use of the Wigner-Eckart theorem, which states that the matrix elements of the dipole operator (or any tensor operator) will obey the following[37]:

$$\langle \alpha', j'm'|T_q^{(k)}|\alpha, jm\rangle = \langle jk; mq|jk; j'm'\rangle \frac{\langle \alpha'j'||T^k||\alpha j\rangle}{\sqrt{2j+1}} \quad (3.45)$$

where j and m are the usual angular momentum labels, and α refers to all other quantum numbers. k refers to the rank of the tensor operator, which, for the dipole operator is 1, and q runs from $-k$ to $+k$, and is the spherical

component of the tensor. The two parts of the left hand part of Eq. (3.45) are the Clebsh-Gordan coefficient, and the so called reduced matrix element of T , which depends only on α, α', j , and j' . What this theorem does is reduce the elements that need to be calculated. In this case, since the only non-angular momentum quantum number in this problem is the principle number, and we are only considering the $2p \rightarrow 3d$ transition, we only need to look at the possible transitions of total angular momentum j of the single particle wavefunctions. Since the electrons in this system are spin $1/2$ particles in either the p ($l = 1$) orbital or the d ($l = 2$) orbital, we have possible transitions from states with $j = 1/2, 3/2$ to $j = 3/2, 5/2$ states. Since T is a rank 1 tensor, the difference in j between the states must be 1 or less, which leaves the only elements that need to be calculated as:

$$\langle j' = 3/2 || T || j = 1/2 \rangle \quad (3.46)$$

$$\langle j' = 3/2 || T || j = 3/2 \rangle \quad (3.47)$$

$$\langle j' = 5/2 || T || j = 3/2 \rangle \quad (3.48)$$

as all others are determined from these three and the relevant Clebsh-Gordan coefficients. These elements themselves are obtained numerically from a Local Density Approximation calculation [23].

The broadening comes from two sources: screening of the core hole (valence electron) by the many-body system, and the finite lifetime of the excitation, which will be taken into account here following [38].

If we re-write the spectral function in terms of t rather than ω , it takes the form, for a given final state f ,

$$F(\omega) = \int_0^\infty dt \exp(i(E_f - E_i)t/\hbar) \langle f(t) | T | i \rangle$$

which, for the case of $|f(t)\rangle = \text{constant}$, reduces to Eq. (3.43). In the presence of screening by the lattice, though, the function $\langle f(t) | T(\omega) | i \rangle$ will decay with

a Gaussian lifetime,

$$\langle f(t)|T|i\rangle = \exp\left(\frac{-D^2 t^2}{2\hbar^2}\right)$$

which, upon the Fourier transform, implies that

$$F(\omega) = \exp\left(\frac{-\omega^2}{2D^2}\right) \quad (3.49)$$

The lifetime of the excitation can be taken as an exponential, so that

$$\langle f(t)|T|i\rangle = \exp\left(\frac{-t}{\tau}\right)$$

which, upon Fourier transform, leaves a Lorentzian,

$$F(\omega) = \frac{\hbar}{\pi\tau} \frac{1}{\omega^2 + (\hbar/\tau)^2} \quad (3.50)$$

Thus, both of these effects can be taken into account from known values for excitation lifetimes and charge screening in the crystal, by broadening the spectrum from eq 3.43 with a Gaussian convoluted with a Lorentzian. As the characteristic times for these processes are known from other work, the Gaussian and Lorentzian broadening can be determined. In this thesis the values used are (FWHM) 1.0 eV and 0.4 eV for the Gaussian and the Lorentzian, respectively[3].

Once the spectrum has been calculated, it is compared to the experimental spectra to determine the χ^2 fit. The parameters in H are then varied systematically, using the Nelder-Mead simplex algorithm to minimize χ^2 and arrive at a set of best-fit parameters.

Chapter 4

Results and Discussion

4.1 NiO

To test the methods described above, we examine NiO, for which the literature provides a wealth of data and theory, and for which we expect the XAS to be clean, without contaminating spectra from displaced Ni ions, due to the relative ease in synthesizing the high quality samples of this compound.

The two methods discussed for taking into account the crystal field potential are identical for NiO, as the symmetry of the crystal is O_h , so there is no approximation needed to reduce the crystal field to one parameter.

The spectrum of NiO is seen to be a good fit with calculations that assume a d^8 occupation of the $3d$ orbital. Using XTLS 8.30, with a fitted O_h crystal field symmetry, we vary U , $10Dq$, Δ , and $(pd\sigma)$ to fit the measured data, taken from [3]. Minimizing the error between the calculated spectrum and experiment results in the parameters listed in Table 4.1. Looking at Fig. 4.1, we see that the procedure reproduced the qualitative features of the spectrum quite well. Comparing values we obtained with those cited in the literature, Table 4.1, we see that the values listed are reasonable.

We might expect that the Coulomb repulsion energy will depend solely on the Ni ion and be fairly insensitive to the specific environment, so that we should keep that fixed throughout the calculations; however, determining this

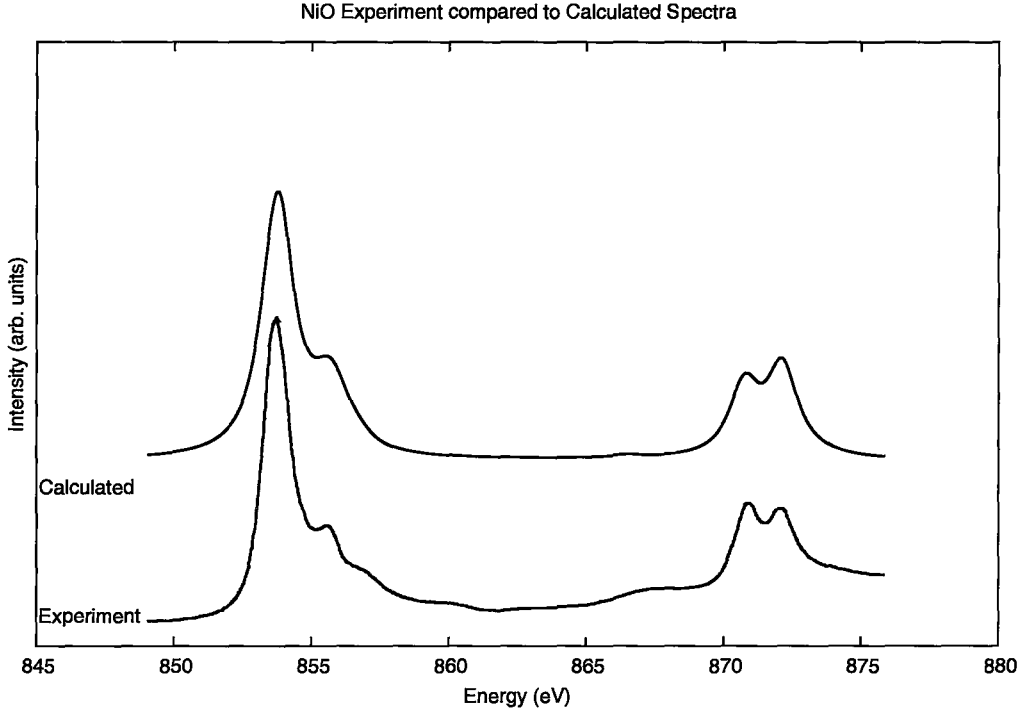


Figure 4.1: Measured NiO XAS from [3], and calculated spectrum from this work. The features of the experimental spectrum are well reproduced in the calculated spectrum.

	$10Dq$	U	Δ	$(pd\sigma)$	ζ_p
This work	1.0	6.0	5.0	1.7	11.33
[36]		6.8	5.2	1.3	
[39]		5.0	4.6	1.0	

Table 4.1: Parameters obtained for NiO in this thesis, with comparison to parameters obtained by other groups on the same compound. All values given in eV.

value from the NiO spectrum is problematic. The problem is that, for a wide range of energies of U and Δ , the $d^{10}\underline{L}^2$ state is energetically removed from the problem, leaving the two states d^8 and $d^9\underline{L}$. But, when only considering two states, the only relevant energy is Δ , and U does not play a large role. Thus the spectrum contains limited information about U , which is born out in calculations in Fig. 4.2, which vary U over a range of 2 eV.

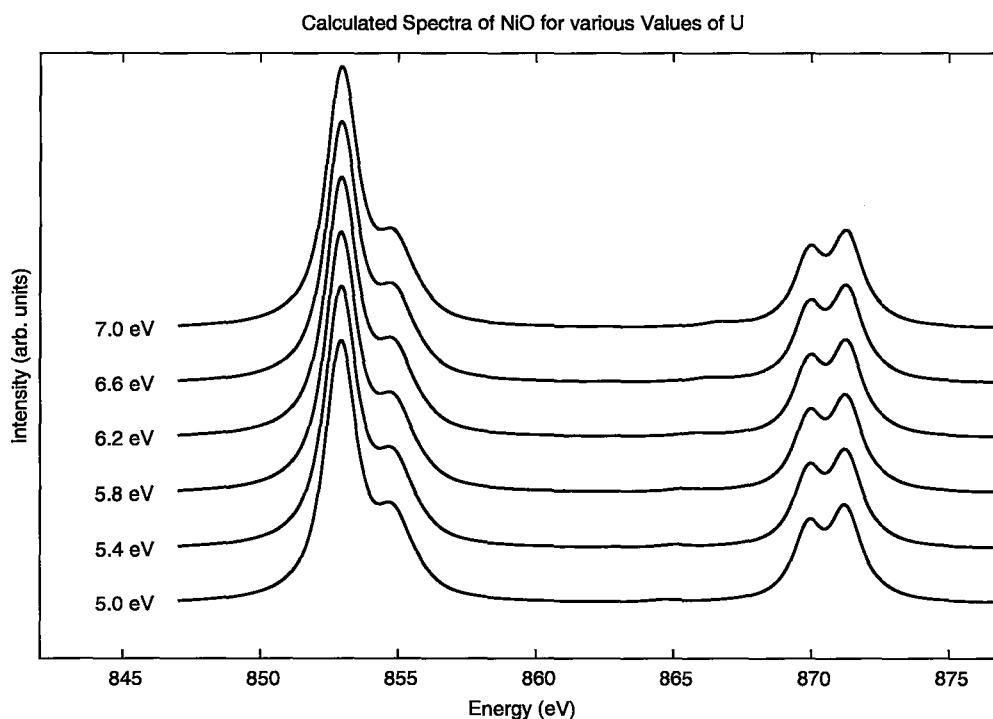


Figure 4.2: Calculated spectra for NiO for different values of U , illustrating the difficulty in using the spectrum to determine values for U .

The charge transfer energy is a function of several things. Primarily, it reflects the electronegativity of the O ion, the Ni ion, and, to a lesser extent, the external potential from the surrounding ions. The external potential could be addressed in an approximate way by performing a Madelung sum over the infinite crystal within a point charge model, but as the most important effects are almost certainly the short range and quantum in nature, it is unclear if this is of any value. The electronegativity is not typically calculated. What a “reasonable” difference in Δ between NiO, LiNiO₂, and NaNiO₂ is, is then

difficult to determine. This will be taken up again in section 4.4.

For NiO, once again the value of $(pd\sigma)$ is difficult to determine with accuracy, due to the fact that the $d^9\bar{L}$ state is removed in energy from the energies of the hopping terms. As we can see in Fig. 4.3, the spectrum is insensitive to changes in the hopping parameters.

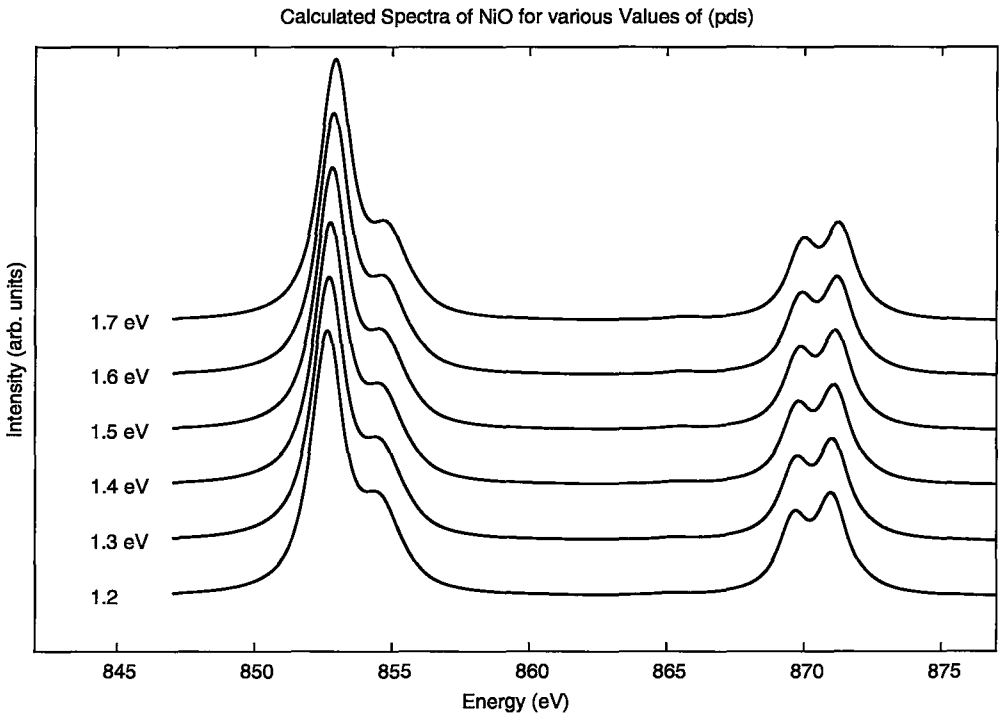


Figure 4.3: Calculated spectrum for NiO for varying values of $(pd\sigma)$. As in the previous figure, we see that the spectrum is insensitive to changes in parameters over a wide range.

So, while one might be tempted to think that NiO would provide a basis for parameters for further calculations, this is hampered by the fact that the spectrum is sensitive to two important parameters: the total energy of the $d^9\bar{L}$ state, given by Δ , and, to a lesser extent, the crystal field splitting $10Dq$.

Energy (eV)	$ xy\rangle$	$ 3z^2 - r^2\rangle$	$ yz\rangle$	$ xz\rangle$	$ x^2 - y^2\rangle$
-0.190	0.832	0	-0.554	0	0
-0.165	0	0.778	0	-0.370	-0.507
-0.053	0	0.062	0	-0.759	0.649
0.052	0	0.625	0	0.536	0.567
0.355	-0.554	0	-0.832	0	0

Table 4.2: Results of the Madelung sum calculation for NaNiO_2 . This symmetry here is lower than cubic, and the intra- e_g and t_{2g} splitting is of the same order as the inter- splitting. This calls into question the validity of the point charge model used in the Madelung sum

4.2 NaNiO_2 - Describing the Jahn-Teller Distortion

We reproduce the spectrum by a calculation that explicitly takes into account the Jahn-Teller distortion of NaNiO_2 . This can be done using the CI software available. The method of using the Ewald sum to find expressions for the terms Eq. (3.12) was employed, producing Table 4.2. Unfortunately, this procedure does not allow the experimental spectrum to be reproduced. Why this is will be discussed below. The approximate symmetry D_{4h} , allowing two free parameters to vary (the total splitting, and the e_g splitting induced by the Jahn-Teller distortion) can reproduce the spectrum calculated via the Ewald sum (fig 4.4), giving confidence that this is an acceptable approximation, as well as the experimental spectrum for NaNiO_2 (fig 4.6).

Thus, the transition was modeled as $O_h \rightarrow D_{4h}$, which is expected to be a reasonable approximation, as the energy splitting is a much more important effect than the eigenstate mixing that is ignored in this approximation. To test this, the spectrum generated by the Ewald sum technique was compared with a spectrum assuming D_{4h} symmetry, with the energy levels taken from the Ewald sum. Having done this, we can compare the calculated spectrum for different Jahn-Teller splittings of the e_g states, with the spectrum for NaNiO_2 , and also that of PrNiO_3 , from [40], a Ni^{3+} compound that does not undergo a Jahn-Teller distortion. This provides strong evidence that the height of the

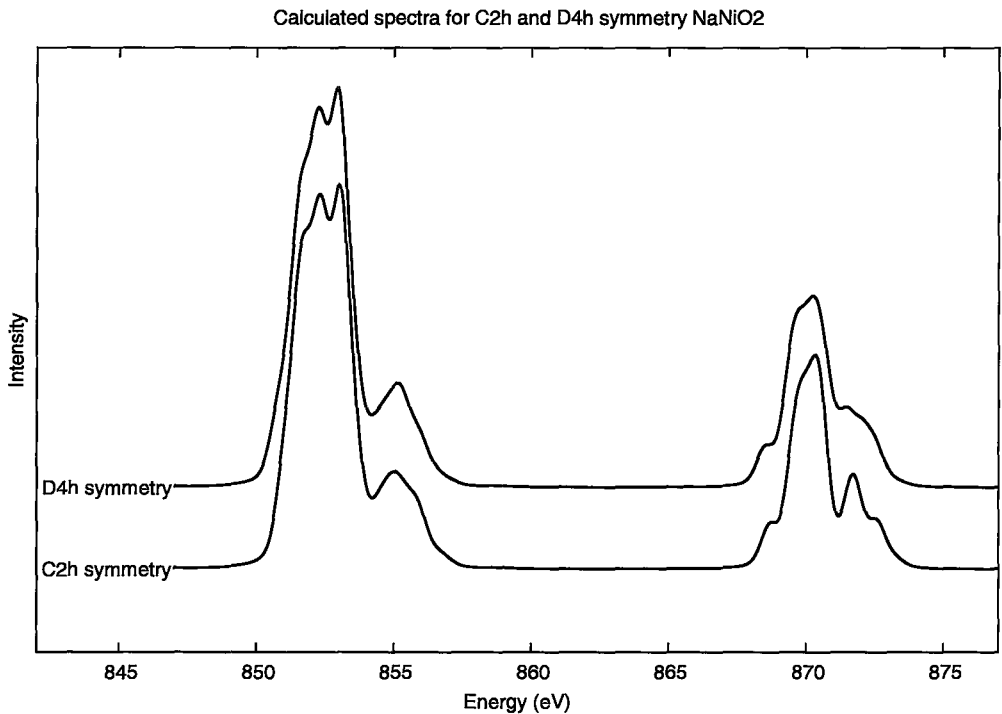


Figure 4.4: Calculations for NaNiO₂ for the actual symmetry (via the Ewald sum of the terms in Eq. (3.12)) and for the approximate D_{4h} symmetry. The Ewald summation does not do a good job of reproducing the spectrum here, while the approximate symmetry can reproduce the actual symmetry calculation, as well as the experimental spectrum (see fig 4.6)

lower energy peak is a function of the orbital order in the system.

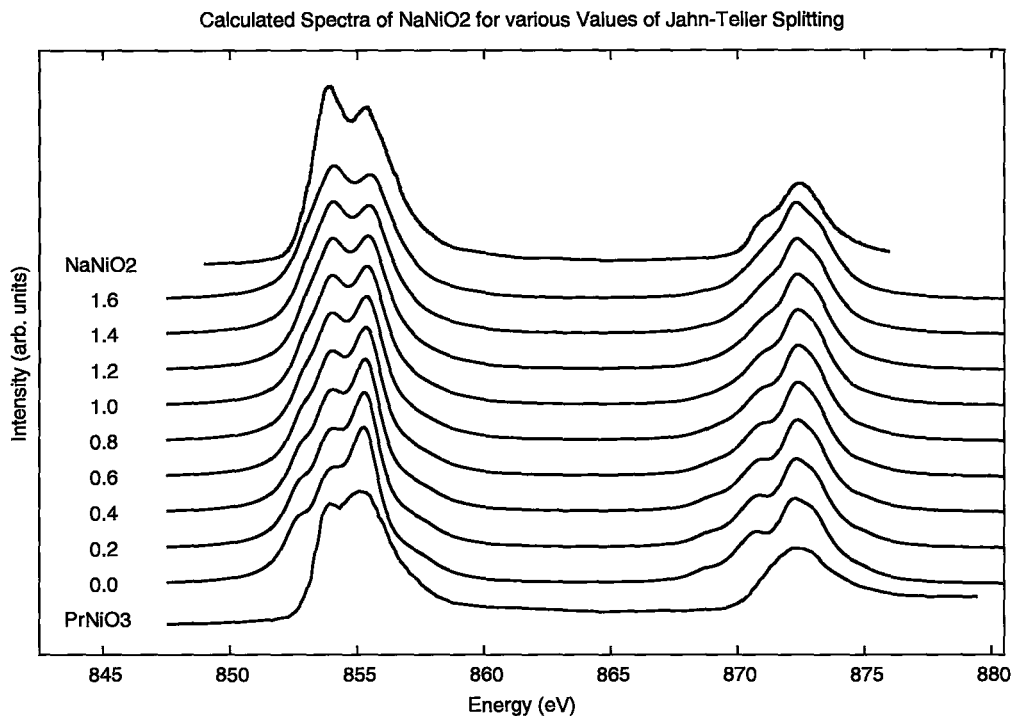


Figure 4.5: XAS for NaNiO_2 , with a e_g splitting from 0 to 1.6 eV. This splitting is much larger than that explained by the crystal field. This can be compared with the XAS for PrNiO_3 , the features of which look more like the undistorted spectrum.

The reader will note, however, that the e_g splittings listed in Fig. 4.5 are too large to be accounted for by the crystal field effects of the physical distortion of the surrounding ions. This points to cooperative effect of

the orbital ordering – we are only using 1 Ni ion and surrounding ligand orbitals, when the real Ni ion is surrounded by six nearest neighbour Ni ions. In the ordered state, then, the energy levels of the orbitals will be determined not only by the crystal field, but by the orbital exchange coupling between the Ni site and the six NN Ni sites. Thus we can view the crystal field as an effective parameter, which, for the e_g splitting, is dominated by a mean field contribution from the orbital Ni-Ni superexchange interaction.

To estimate, then, the effective splitting that the orbital states will have in

$10Dq$	JT splitting	$(pd\sigma)$	$(pd\pi)$	U	Δ	ζ_p
1.5	1.5	1.7	-0.77	6.0	13.2	11.89

Table 4.3: Parameters determined for NaNiO_2 by providing best fit between calculated and experimental spectrum

the ordered state, we can use the orbital exchange coupling from [9]:

$$J_T = -\frac{2t^4 U_p}{\Delta^3(2\Delta + U_p)} \quad (4.1)$$

which, when we put in the values we have for Δ and t , and use the value for U_p estimated in [4], gives $J_T = 0.06$, which, for 6 nearest neighbour ions, gives an effective splitting of 0.72 eV. With a crystal field splitting of 0.3 eV, this gives a total effective splitting of 1.0 eV, which is still smaller than what is found for the spectrum. However the point charge model is expected to be least accurate in determining the magnitude of the e_g splitting, so there is a fair bit of error in the estimated crystal field splitting. So the crystal field in this case is a combination of the physical crystal field resulting from the coulomb potential of the ions in the crystal lattice, and an effective potential resulting from the orbital exchange interaction with the surrounding Ni ions in the orbitally ordered state. An interesting thing to note here is that the crystal field is actually smaller than the orbital exchange contribution; thus we can assume that the exchange pathways between Ni sites are more important in determining the orbital ordering than the symmetry breaking of the local environment. The hopping is assumed to be unaffected by the distortion.

The parameters in Table 4.3 are those which produce the best fit between the measured spectrum and the calculated spectrum. Here, Δ is larger than U by 5.2 eV, which represents the energy of the $d^8 \underline{L}$ state above the d^7 ground state. The spectrum, though, is somewhat insensitive to changes in Δ and $(pd\sigma)$, as seen in figs. 4.7. This is a consequence of the fact that the spectrum is most sensitive to the orbital ordering, as seen above, so that a certain amount of mixing with the $d^8 \underline{L}$ state, the magnitude of which is determined by the parameters Δ and $(pd\sigma)$, will not change the overall shape significantly. To

pursue this further, we can examine two spectra with very different values of the Ni occupation. In Fig. 4.8, we have a calculated spectrum with a Ni $3d$ occupation of 7.25, which results from the parameters listed in Table 4.3, and another in which we have removed all states except the d^7 state, thus forcing a $3d$ occupation of 7.0. The spectrum are the same, illustrating that the spectrum is insensitive to the presence of the $d^8\bar{L}$ state.

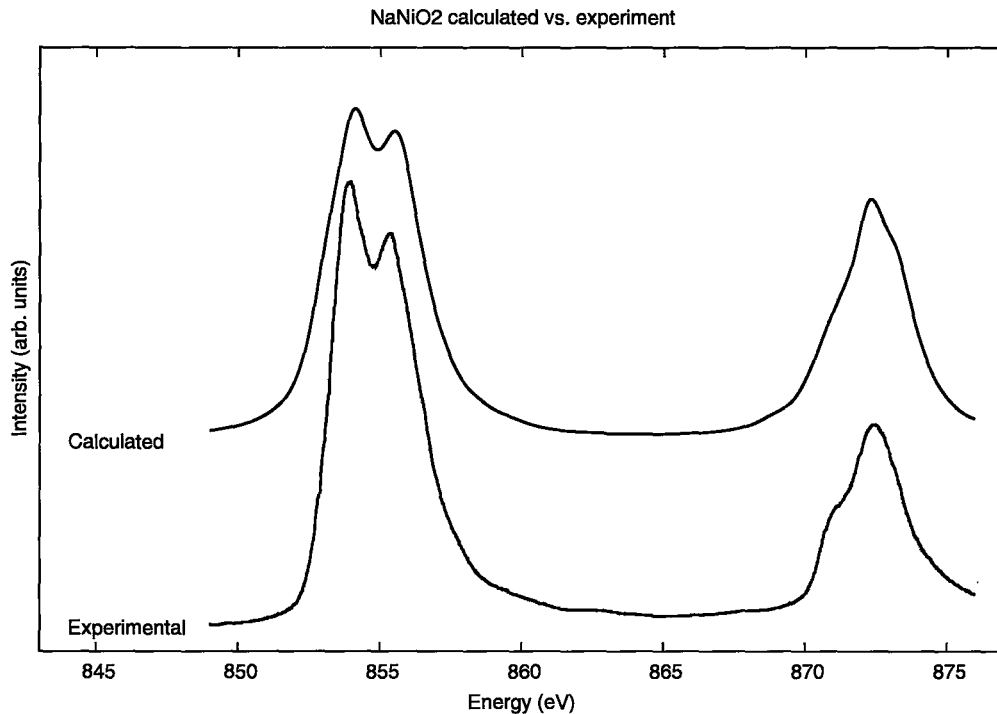


Figure 4.6: Final calculated spectrum for NaNiO_2 , compared to experimental data from [3].

4.3 LiNiO_2 - Determining the Formal Valency

The XAS presented here has a different shape than that of other groups. The two spectra are compared in Fig. 4.11, and while the TEY spectrum matches with that obtained in [3, 6], shown in Fig. 4.10, the TFY spectrum, which we expect to be a better probe of the bulk sample, is significantly different.

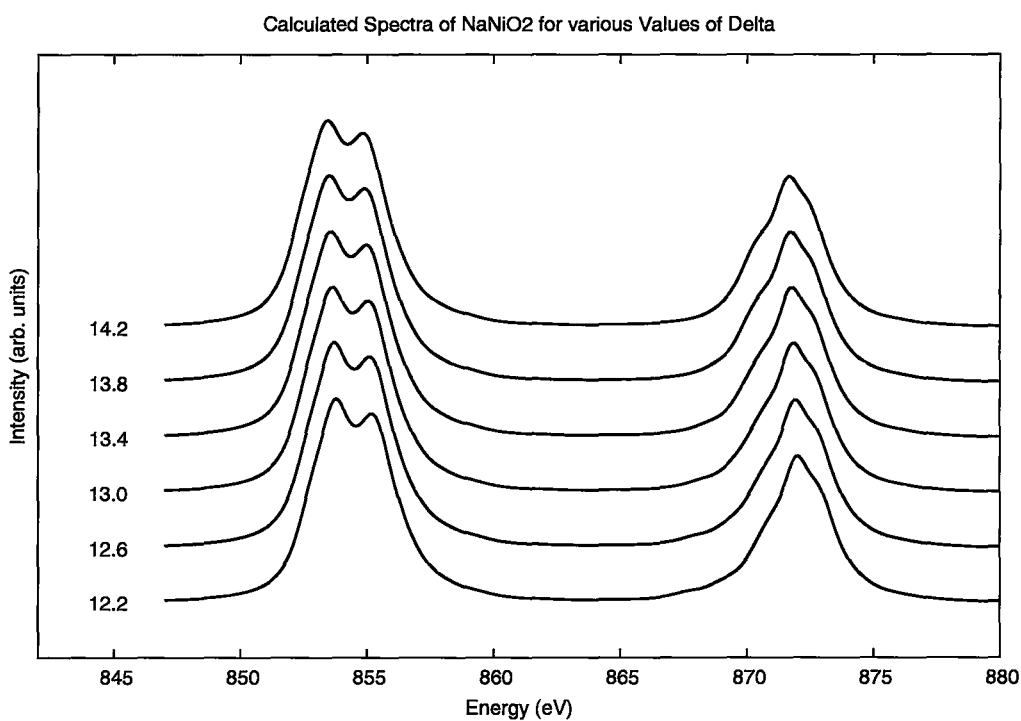


Figure 4.7: NaNiO₂ spectra for various values of Δ . Of particular interest is the movement of the shoulder peak of the 872 eV feature.

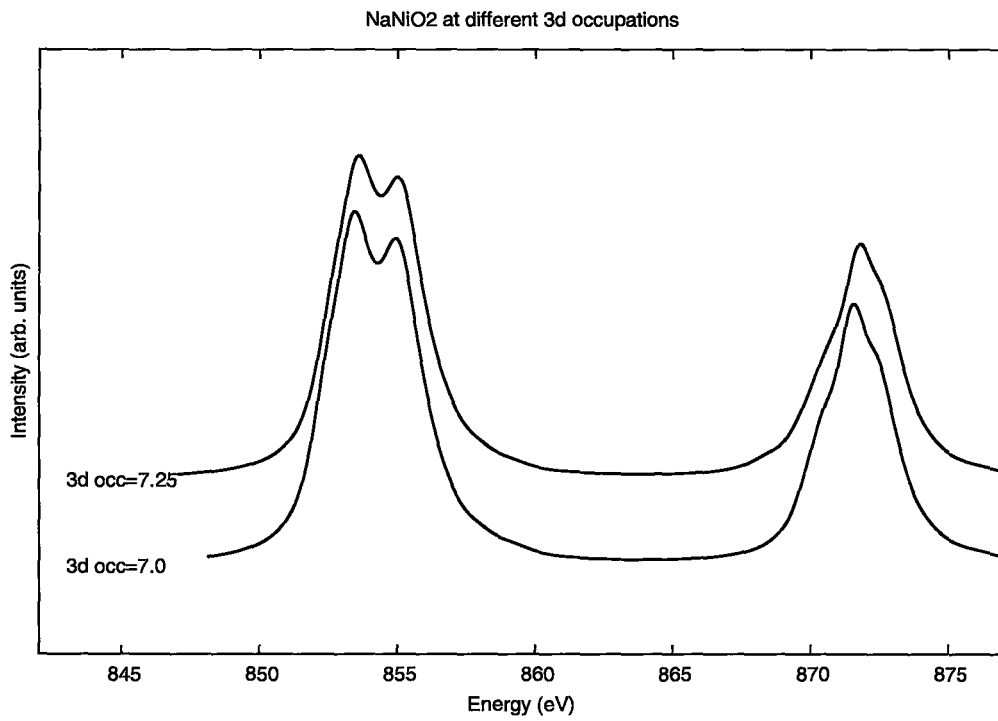


Figure 4.8: Calculated NaNiO₂, with and without inclusion of the d^8 state, which raises the $3d$ occupation.

In addition, one can also note that the spectrum here is not a combination of spectra for NiO and NaNiO_2 , or even other Ni $3+$ low-spin compounds such as PrNiO_3 , as suggested in [6, 22]. Instead, the shape of the spectrum cannot be reproduced by a linear combination of d^7 and d^8 spectra.

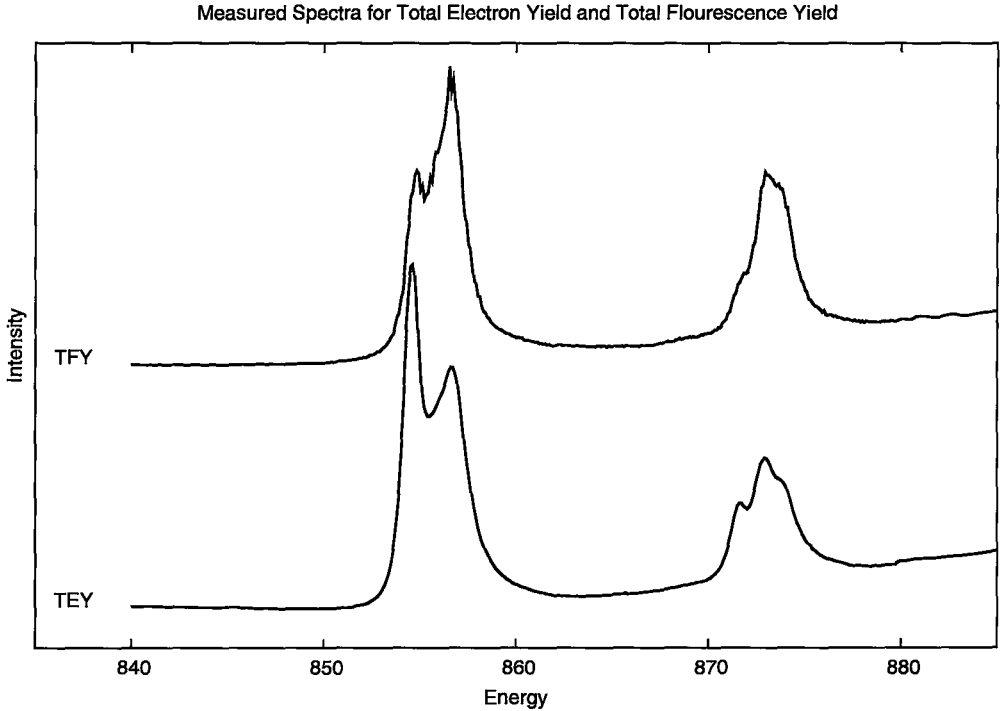


Figure 4.9: XAS data obtained via TEY and TFY measurements, for comparison to Fig. 4.11

The procedure outlined in sec. 3.4 produced the calculated spectrum in Fig. 4.11, produced from the parameters listed in Table 4.4, which is compared to the experimental spectrum. One can immediately see that the calculated spectrum does not reproduce the features of the measurement as well as for the previous two compounds. This will be discussed below.

$10Dq$ Ni	$10Dq$ ligand	U	Δ	$(pd\sigma)$	$(pd\pi)$	ζ_p
0.7	-0.6	6.0	5.6	1.95	-1.25	11.49

Table 4.4: Best fit parameters for LiNiO_2

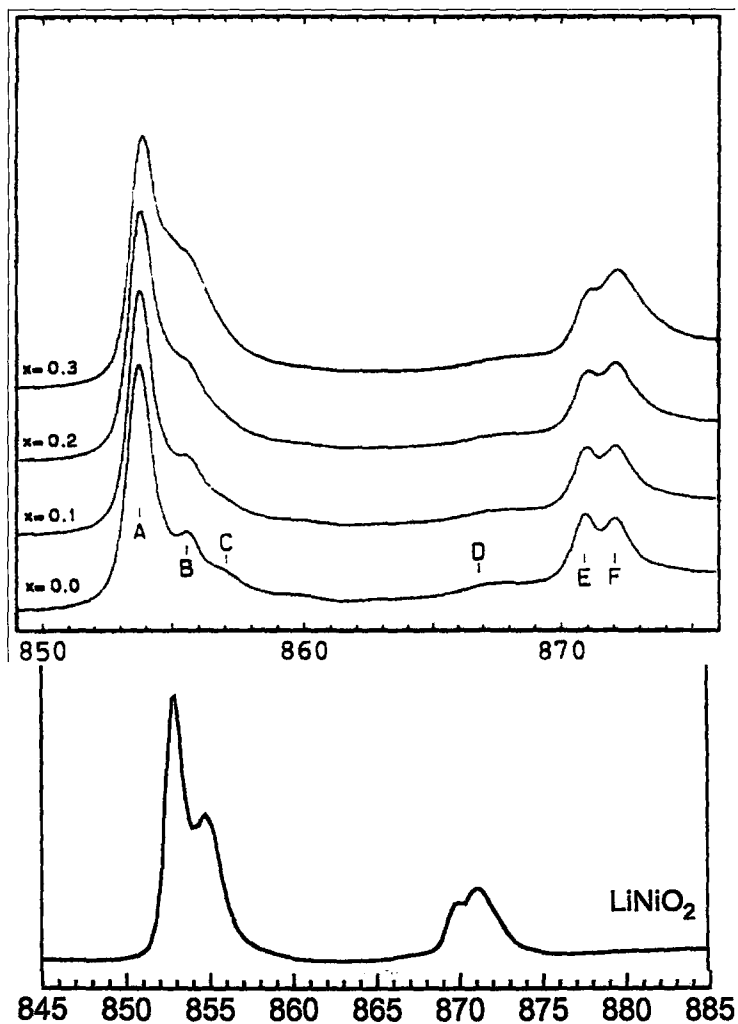


Figure 4.10: XAS obtained by [3], [6]. These data, which are TEY data, are consistent with the TEY data obtained here, and hence different than the TFY data that is a more accurate probe of the bulk electronic structure.

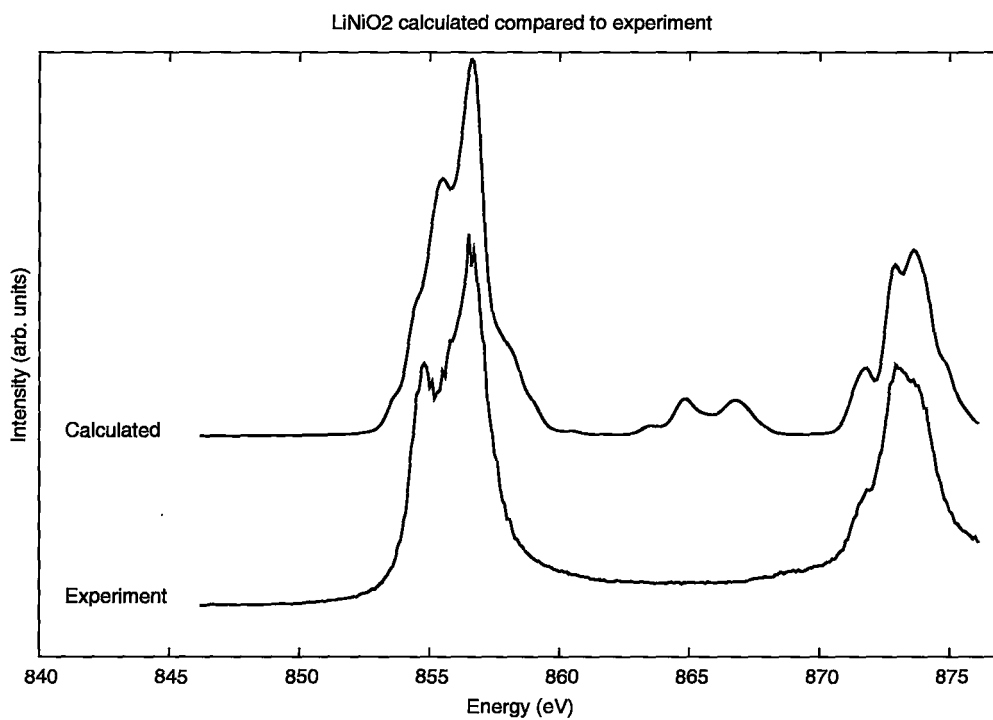


Figure 4.11: Calculated and Experimental spectra for LiNiO₂. The qualitative features are reproduced, although less accurately than for NiO and NaNiO₂.

To reproduce the spectrum here, a very small Ni $10Dq$ ($< 0.1\text{eV}$) was necessary. This could be the result of the large hybridization with the O $2p$ states, as those states are in a crystal field whose splitting we expect to be opposite to that of the Ni site. Indeed, including a negative splitting on the ligand orbital has the same effect on the calculated spectrum as a vanishing splitting on the Ni site, shown in Fig. 4.12. In addition, the magnitudes for $(pd\sigma)$ and $(pd\pi)$ are at the very high end of what is reasonable given the corresponding values for NaNiO_2 and standard procedures for estimating these values. However, given the fact that the effective crystal field splitting has been reduced by the hybridization, lowering the magnitude of the hopping elements would result in a high-spin state for the Ni ion, and a spectrum that is certainly not correct, in addition to conflicting with other experimental evidence about the compound [25].

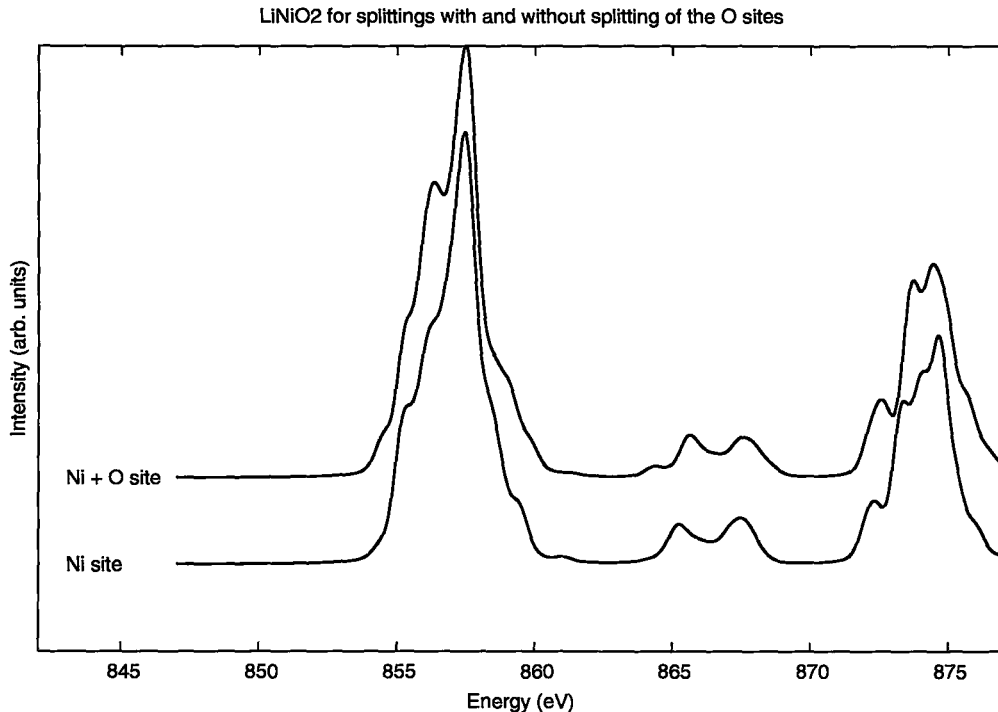


Figure 4.12: Calculated spectrum for LiNiO_2 for the case of $10Dq = 0$, and for the case of a splitting of 0.7 eV on the Ni site and -0.6 eV on the ligand site.

The most obvious deviation of the calculated spectrum from the experi-

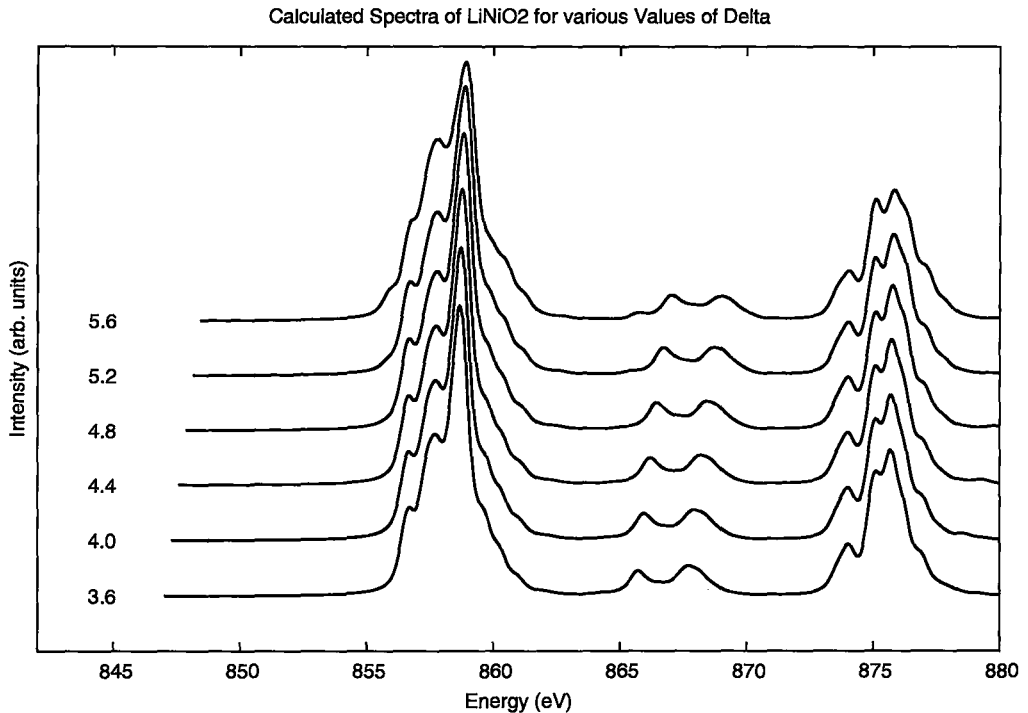


Figure 4.13: LiNiO_2 vs. Δ . The movement of the feature between the two main peaks is what is of interest here. As expected, it is somewhat sensitive to Δ .

mental is in the feature at 865 eV, which is not seen at all in the experiment. This feature appears in other XAS calculations [41], and is expected to be dependent on Δ , as shown in Fig. 4.13. If then, one assumes that the spectrum consists of a sum of Ni ions in slightly different environments, due to the exchange of Ni and Li ions which is known to take place in this compound [15], then the addition of these spectra could smear out features between the two main peaks, while the features in the main peaks do not change and would be unaffected. Whether this is actually the case is difficult to determine.

One issue with the parameters and spectrum presented here is that the hopping parameters are larger than those for comparable compounds [23, 36]. An argument for why they are large here is as follows: The splitting (or effective splitting) on the Ni site must be small to give even a qualitative fit to the data, as seen in Fig. 4.14. That being the case, the hopping values found here are

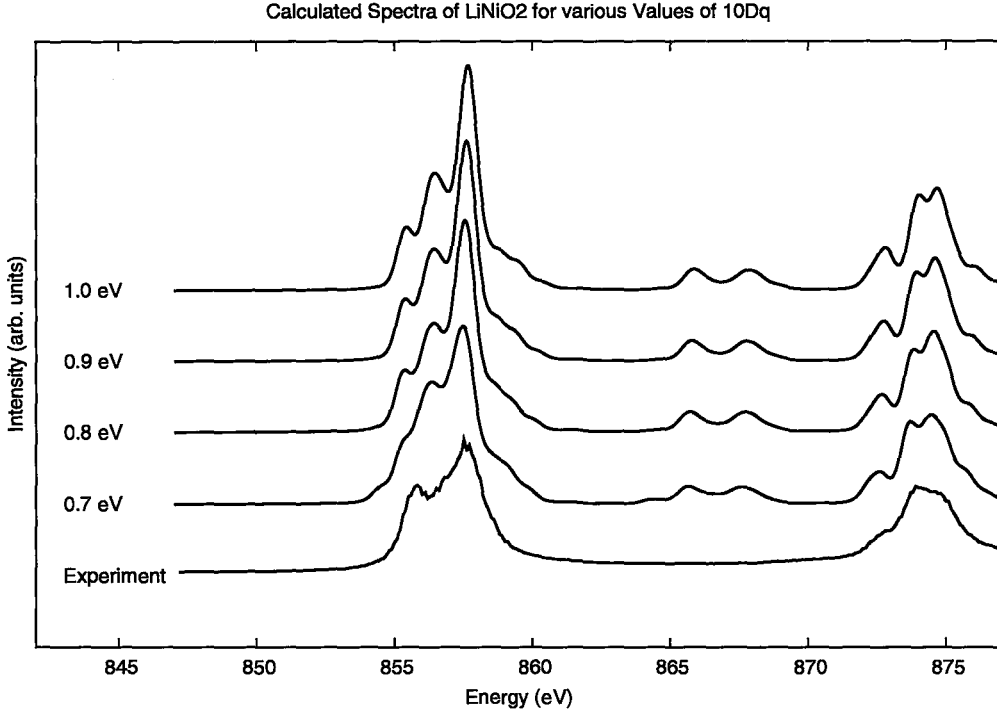


Figure 4.14: LiNiO₂ vs. $10Dq$. What is seen here is that the features of the 857 eV peak change as a function of $10Dq$, with a second shoulder peak at lower energy emerging as $10Dq$ is increased.

the smallest that will keep the system in the low spin configuration, as the effective splitting from the crystal field and the hopping terms must be larger than the Hund's coupling, which favours the high spin state.

Given that the hybridization is large, one question that can be asked is whether the assumption of a single ion surrounded by a ligand orbital is justified. The O $2p$ band in Eq. (3.2) is assumed to be flat, however obviously this is not actually the case, and we might expect effects coming from the $2p$ band structure to play a role in a system with a large degree of hybridization. Since, throughout a series of fits, the experimental spectrum is only reproduced with even qualitative accuracy for parameters that lead to a hybridized state with a mostly $d^8 \underline{L}$ character, we can conclude that hybridization is essential for describing the spectrum of this compound. The features in the spectrum that are not reproduced in the experiment may be artifacts of the assumptions about the

2p band structure.

In addition to the Ni L edge, one can examine the O K edge spectrum, in which the absorption process is one of exciting an electron from the O 1s shell to the lowest levels above the fermi surface. The spectrum here is much broader than that of the Ni L edge, as might be expected when exciting the electron into a conduction band rather than a localized orbital, but the feature we are interested in is whether we see a O 2p hole immediately below the conduction band spectrum. This feature was observed for the series $\text{Li}_x\text{Ni}_{1-x}\text{O}$ in [4, 5] at 528-530 eV, reproduced here in Fig. 4.15.

4.4 Comparison of NaNiO_2 and LiNiO_2

To summarize, the XAS of NaNiO_2 is well fitted by a calculation which predicts the Ni to be in the low spin, d^7 state, in the presence of a Jahn-Teller distortion. This is consistent with other studies of NaNiO_2 . In addition, the spectrum calculated here is dependent on the Jahn-Teller distortion in a way that can be measured. LiNiO_2 , on the other hand, cannot be fit by either a d^7 spectrum or a d^8 spectrum, or some linear combination of the two. LiNiO_2 requires a strongly hybridized state to achieve even qualitative agreement between the calculated spectrum and the experimental spectrum. This result is clear from the new XAS data presented here, which are qualitatively different than that used in [3, 6, 22].

Since there is a higher valency in LiNiO_2 , we expect that the energy gain from a Jahn-Teller distortion will be reduced. To quantify this, we compare the energy gain for a small distortion of the ground state for the parameters for LiNiO_2 and NaNiO_2 , Fig. 4.17. The slope of the energy vs. distortion at 0 distortion is a factor of ten larger in magnitude for NaNiO_2 than for LiNiO_2 . Since the distortion costs energy by moving the ions from their equilibrium position, this difference in energy explains the lack of distortion in LiNiO_2 .

One can now ask the question, what is different between the two materials. The slightly closer distance of the Ni-O bonds in LiNiO_2 compared to NaNiO_2

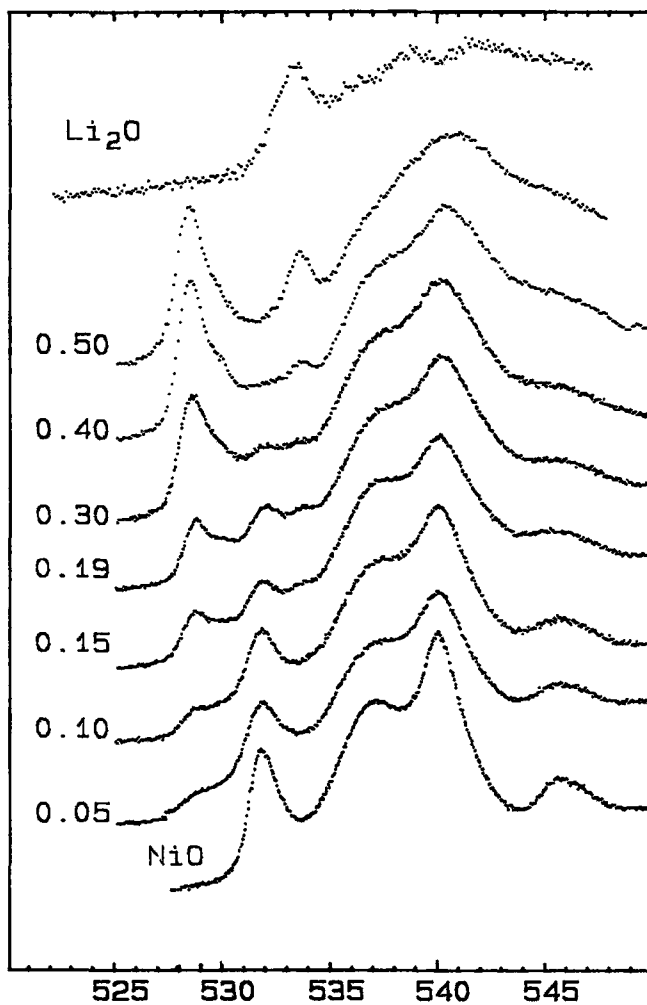


Figure 4.15: O K edge data from [4]. One can clearly see the feature opening up at 528-530 eV, below the conduction band spectrum, that is indicative of a hole on the O 2p orbital

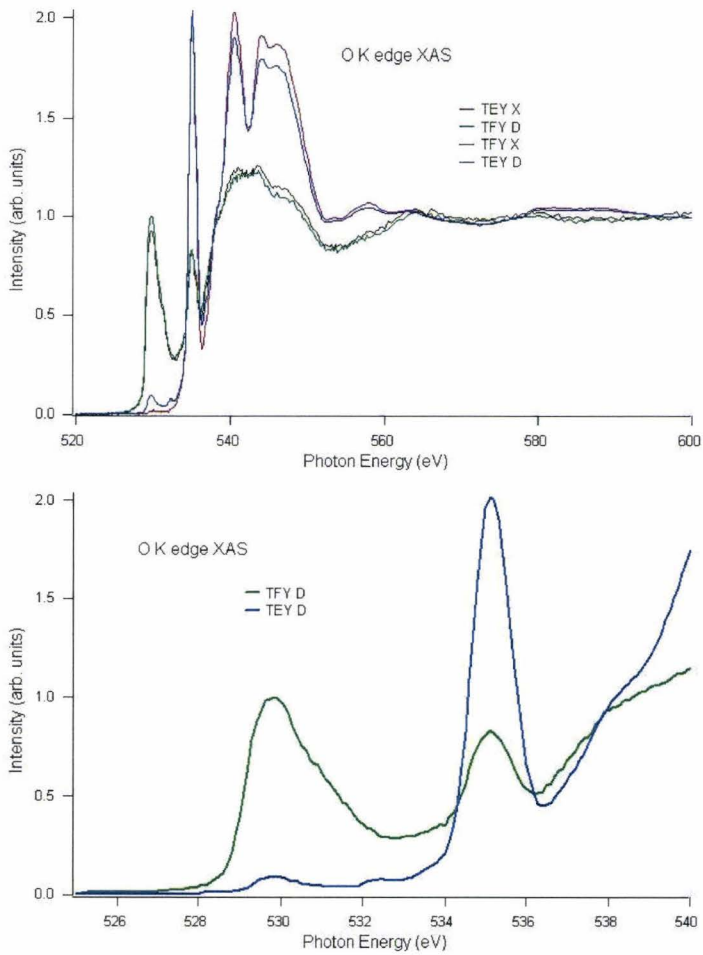


Figure 4.16: O K edge data from this work. The feature at 530 eV observed in Fig. 4.15 is present in the TFY data, indicative of a hole on the O 2p shell.

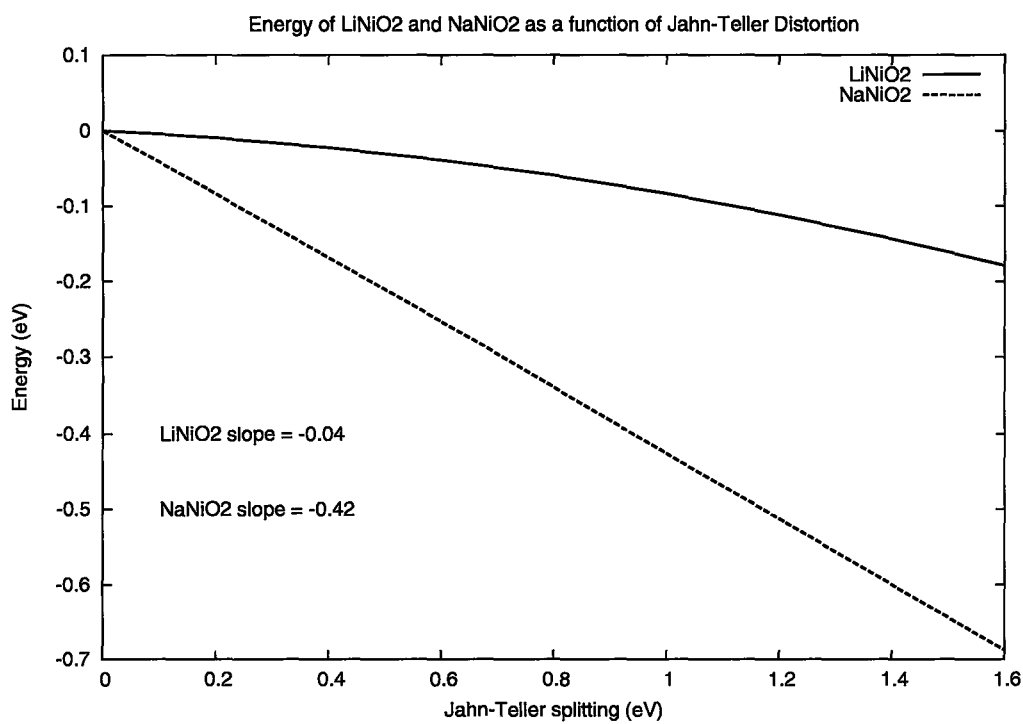


Figure 4.17: Energy of the ground state as a function of Jahn-Teller distortion. The slope at 0 distortion is given, it is a factor of 10 larger for NaNiO₂ than for LiNiO₂.

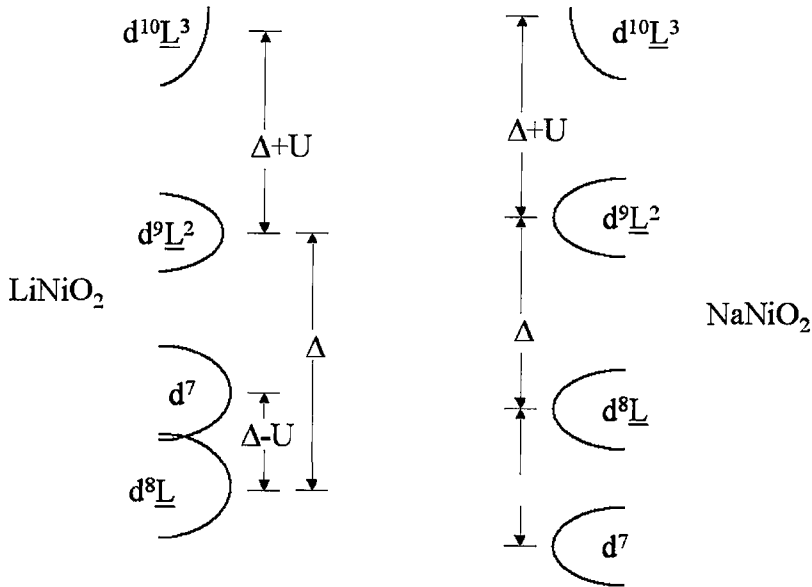


Figure 4.18: Diagram of NiO , NaNiO_2 , and LiNiO_2 , illustrating the effect of $\Delta < U$

makes the overlap integrals ($pd\sigma$) and ($pd\pi$) slightly larger in magnitude for LiNiO_2 , which has some impact, but the biggest difference seems to be the value of Δ . Ascribing this as the “cause” of the difference in formal valency, and hence in orbital ordering, is somewhat problematic, as Δ is a phenomenological parameter, and hence we don’t know what underlying physical processes drive the difference between the two materials. In this analysis, Δ emerges through process of elimination; the difference in materials must be due to Δ as the hopping parameters and U cannot be very different, and the crystal field does not affect the spectrum or the valency enough to be of much impact. Optical absorption measurements comparing LiNiO_2 and NaNiO_2 above and below the Jahn-Teller transition in NaNiO_2 at 480 K may yield more information as to the intrinsic differences between these materials.

4.5 Future Work

Susceptibility and neutron scattering measurements on LiNiO_2 show that the magnetic spins are spin $1/2$. Thus, if Ni is in a spin 1 state with a spin $1/2$ hole on the surrounding O, the Ni spin and the hole must be coupled antiferromagnetically in a doublet state, reminiscent of the Zhang-Rice singlet in the cuprates, in which a spin $1/2$ on the Cu^{2+} forms a singlet with a hole on a neighbouring O ion. The strength of this coupling is estimated in [4] to be on the order of 0.5 eV, thus determining the splitting between the total spin $1/2$ and spin $3/2$ states. This splitting may be observable in high energy inelastic neutron scattering. In addition, the large direct Ni-O exchange will dominate the effective interaction between the spin $1/2$ magnetic moments. The nature of the effective Ni-Ni exchange will depend crucially on the interaction between the O holes. In Fig. 4.19 two possibilities are illustrated, showing how the Ni-Ni interaction between a given pair may be mediated by either one or two hole occupied O sites. An interaction mediated by two O holes is shown schematically in Fig. 4.20, illustrating the important role the O-O interaction has.

Another interesting possibility arises from the fact that the presence of holes on the O sites may distort the lattice. The lattice distortion may be able to explain the local distortion observed in [18, 25].

Additionally, each Ni spin-1 site will, on average, have 3 nearest neighbour O spin $1/2$ holes, any one of which can couple to form the spin- $1/2$ doublet. If several coupling arrangements are degenerate, as shown schematically in Fig. 4.21, this can lead to RVB type physics in LiNiO_2

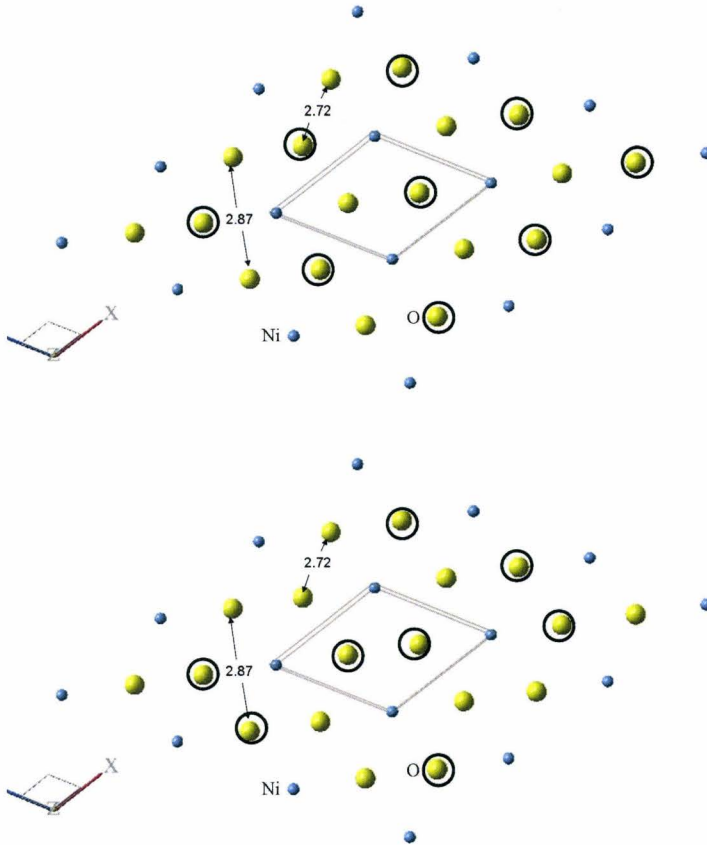


Figure 4.19: Schematic of possibilities for the occupied O sites. The ground state will depend on the nature of the hole-hole nearest neighbour interaction on the O sites.

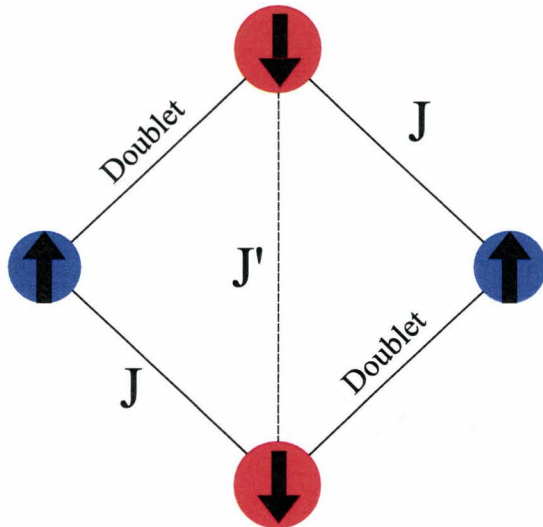


Figure 4.20: Schematic of couplings in a Ni_2O_2 plaquette, mediated by two spin-1/2 holes on the O sites. The interaction J' is important here and its nature is unknown.

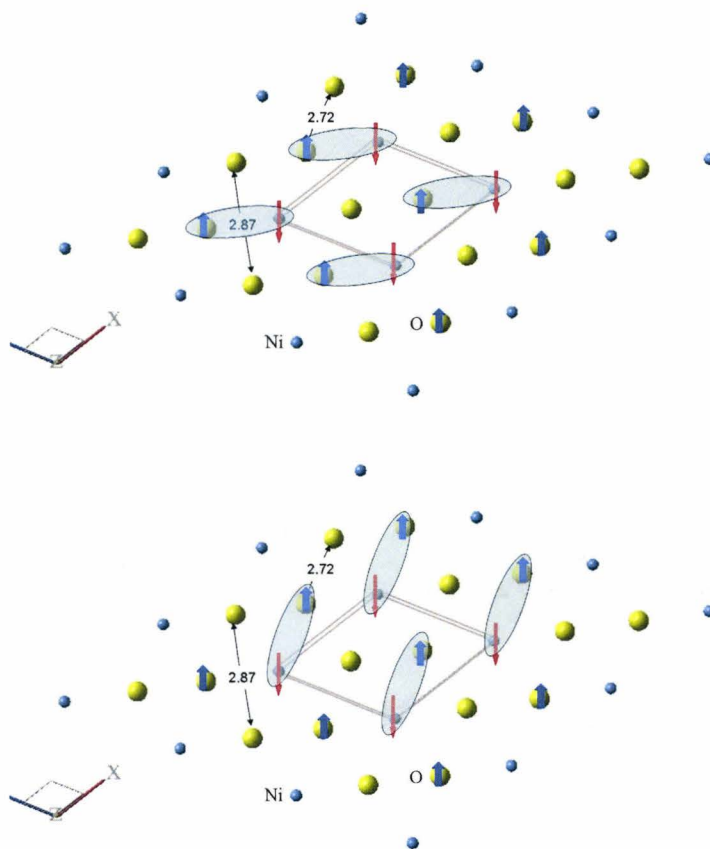


Figure 4.21: For a given ground state O hole occupation, there is the degeneracy of doublet formation between the spin on the Ni and the spin on the O

Chapter 5

Conclusions

We have examined XAS data for NiO, NaNiO₂, and LiNiO₂, both published and unpublished, using configuration interaction software XTLS 8.30, while varying parameters to find χ^2 best fit values. The NiO spectrum was found to be insensitive to all but two parameters, making it less ideal for establishing a baseline than had been hoped. It has been determined that NaNiO₂ spectrum is well described by a d^7 state, with the presence of a Jahn-Teller distortion that induces an orbital ordering. The spectrum of LiNiO₂ cannot be described by a linear combination of d^7 and d^8 spectra, in contrast to previous work on the subject. LiNiO₂ displays features described by a large degree of hybridization between the Ni 3*d* orbitals and the O 2*p* orbitals. This suggests several promising avenues for theoretical and experimental work, with the possibility of a quantum liquid state in LiNiO₂, and calls for more work on the interaction between the O 2*p* holes.

Appendix A

The Ewald Sum

To evaluate the crystal field, we must consider a sum of the type

$$\sum_{\vec{d}} \sum_{\vec{R}} \left(\frac{Q_{\vec{d}}}{|\vec{R} - \vec{d}|} \right)$$

to evaluate the Coloumb potential from every atom in the crystal, where \vec{d} is summed over all atoms in the unit cell, \vec{R} over every lattice position in all space, and $Q_{\vec{d}}$ is the charge of the ion. The sum of $Q_{\vec{d}}$ is zero, since the crystal is electrically neutral. Unfortunately, this sum is conditionally convergent, which presents two problems: the sum will converge slowly, and, worse, can be made to converge to any value by choosing a suitable ordering of summation. The fact that the sum can be made to converge to any value can be viewed physically as assigning the crsytal a net surface charge; different orderings of the summation correspond to different surface charges, and hence different crystal potentials. Fortunately, Ewald's method will allow us to address both these issues by recasting the sum as an absolutely convergent one. Here we follow [42] and [43] in the derivation of the Ewald sum. To start, we note that

$$\sum_{\vec{R}} \frac{1}{|\vec{d} - \vec{R}|} = \sum_{\vec{R}} \frac{2}{\sqrt{\pi}} \int_0^{\infty} e^{-\rho^2(\vec{d} - \vec{R})^2} d\rho = \int_0^{\infty} d\rho \frac{2}{\sqrt{\pi}} \sum_{\vec{R}} e^{-\rho^2(\vec{d} - \vec{R})^2}$$

Now we take

$$\frac{2}{\sqrt{\pi}} \sum_{\vec{R}} e^{-\rho^2(\vec{d}-\vec{R})^2}$$

and see that it must be periodic in \vec{R} . Thus we can express it in terms of the reciprocal lattice by means of a Fourier transform:

$$\frac{2}{\sqrt{\pi}} \sum_{\vec{R}} e^{-(\vec{d}-\vec{R})^2\rho^2} = \sum_{\vec{K}} F_{\vec{K}} e^{-i\vec{K}\cdot\vec{d}} \quad (\text{A.1})$$

where

$$F_{\vec{K}} = \frac{1}{V} \int \frac{2}{\sqrt{\pi}} \sum_{\vec{R}} e^{-(\vec{d}-\vec{R})^2\rho^2} e^{-i\vec{K}\cdot\vec{d}} d\vec{d} \quad (\text{A.2})$$

and \vec{K} are the reciprocal lattice points, and V is the volume of integration.

We can multiply this by $e^{i\vec{K}\cdot\vec{R}} = 1$ (by the definition of a reciprocal lattice vector) to get

$$F_{\vec{K}} = \frac{1}{V} \frac{2}{\sqrt{\pi}} \int \sum_{\vec{R}} e^{-(\vec{d}-\vec{R})^2\rho^2 - i\vec{K}\cdot(\vec{d}-\vec{R})} d\vec{d}$$

Now, since the integral is over all space, a transformation $\vec{R} - \vec{d} \Rightarrow \vec{d}'$ does not change the value of the integral. Thus, transforming each term likewise,

$$F_{\vec{K}} = \frac{N}{V} \frac{2}{\sqrt{\pi}} \int e^{-d^2\rho^2 - i\vec{K}\cdot\vec{d}} d\vec{d} \quad (\text{A.3})$$

Evaluating this integral gives:

$$F_{\vec{K}} = \frac{2\pi}{v_c} \frac{1}{\rho^3} e^{-K^2/4\rho^2} \quad (\text{A.4})$$

where v_c is the unit cell volume. At this point we note that if we split the integral into two parts, and substitute (A.1):

$$\sum_{\vec{R}} \frac{1}{|\vec{d}-\vec{R}|} = \frac{2\pi}{v_c} \int_0^g \sum_{\vec{K}} \frac{1}{\rho^3} e^{-K^2/4\rho^2 + i\vec{K}\cdot\vec{d}} d\rho + \sum_{\vec{R}} \frac{2}{\sqrt{\pi}} \int_g^\infty e^{-(\vec{d}-\vec{R})^2\rho^2} d\rho \quad (\text{A.5})$$

where g is termed the splitting parameter. For the $\vec{R} = 0$ term in the real

sum, we note that

$$\begin{aligned} \frac{2}{\sqrt{\pi}} \int_g^\infty e^{-d^2 \rho^2} d\rho - \frac{1}{d} &= \frac{2}{\sqrt{\pi}} \int_g^\infty e^{-d^2 \rho^2} d\rho - \frac{2}{\sqrt{\pi}} \int_0^\infty e^{-d^2 \rho^2} d\rho \\ &= -\frac{2}{\sqrt{\pi}} \int_0^g e^{-d^2 \rho^2} d\rho \end{aligned}$$

so that, we have, evaluating the reciprocal space integral in (A.5),

$$S(\vec{d}) = \sum_{\vec{R} \neq 0} \frac{\text{erfc}(g|\vec{d} - \vec{R}|)}{|\vec{d} - \vec{R}|} + \frac{4\pi}{v_c} \sum_{\vec{K} \neq 0} \frac{1}{K^2} e^{-K^2/4g^2 + i\vec{K} \cdot \vec{d}} - \int_0^g \frac{2}{\sqrt{\pi}} e^{-d^2 \rho^2} d\rho \quad (\text{A.6})$$

where

$$S(\vec{d}) = \sum_{\vec{R} \neq 0} \frac{1}{|\vec{d} - \vec{R}|}$$

Since these terms involve e^{-K^2} and $\text{erfc}(R)$, they both converge rapidly. The reason why the $\vec{K} = 0$ term is ignored is that it will be the same for each sublattice, which means that for a neutral unit cell, we will be cancelling it, since our overall sum will be something of the form $S(\vec{d}) - S(0)$. In effect, we have contained all the divergence due to surface charge in the $\vec{K} = 0$ term, and thus by setting it equal to 0 overall, we ensure that our crystal is electrically neutral. Just how fast each term converges is controlled by g ; in general, there is a trade-off between the rate of convergence of the reciprocal space sum and the real space sum. If g is chosen to be on the order of $\frac{1}{R}$, with R the length of a primitive translation vector, then both sums converge quickly. Pursuing a more detailed argument for setting g , we can follow [44] and [45]:

Assume that we want the error in the real sum to fall below some value e^{-p} , where p is a parameter controlling the error. Then, since we expect $\text{erfc}(g \cdot R)$ to behave as $e^{-g^2 R^2}$ for large R , we get

$$\begin{aligned} g^2 R^2 &= p \\ g &= \frac{\sqrt{p}}{R} \end{aligned} \quad (\text{A.7})$$

where R here is the cutoff value for the real space sum.

Since the reciprocal sum terms depend on $e^{-K^2/4g^2}$, we have

$$\frac{K^2}{4g^2} = p$$

$$K = 2g\sqrt{p} = \frac{2p}{R} \quad (\text{A.8})$$

So, eqs. A.7 and A.8 give a relationship between g , R , and K that will hold return a given accuracy e^{-p} for a given real space cutoff R . The calculations here typically used $p = 26$ and $R = 10$, with R in Angstroms and p dimensionless.

It is important to note that the individual terms $S(\vec{d})$ as calculated by Ewald sum do not have any physical meaning on their own. It is only when they are combined to form a electrically neutral unit cell that they acquire the meaning of the electrostatic potential at the origin[42]. This can be seen clearly by noting that $S(\vec{d})$ converges for a lattice composed entirely of, say, positive ions. Yet in reality the energy obviously diverges; essentially we are no longer justified in removing the $\vec{K} = 0$ term. Also of note is that while the final result will be independent of the splitting parameter g (at least in theory), each $S(\vec{d})$ will not[43].

For $l = 0$, we know that the spherical harmonic is

$$Y_0^* = \frac{1}{\sqrt{4\pi}}$$

so we have

$$\sum_{\vec{R}} \frac{1}{\sqrt{4\pi}} \frac{1}{R} = \frac{1}{\sqrt{4\pi}} S(\vec{d}) \quad (\text{A.9})$$

for each sublattice. So this sum is easily evaluated using the Ewald technique. In any case, at $l = 0$, we have that $m' = m''$ is the only term for which the Wigner $3j$ symbols do not go to 0. Further, the Wigner symbols are all equal for $m' = m''$, so the contribution of $l = 0$ to the Hamiltonian matrix is a constant addition to the diagonal elements. It is easily seen that this will shift the eigenvalues by a constant but not affect the splitting between them. Thus

we can ignore the $l = 0$ term when the splitting is what we are after; however, having the capacity to evaluate the $l = 0$ term, which corresponds to the point energy of the atom, is a useful check on the program, since these energies are tabulated for many common crystals[43].

For the $l = 2$ term,

$$\sum_{m=-2}^2 \sum_{\vec{R}} \frac{Y_{2,m}^*}{R^3}$$

we convert the spherical harmonics into cartesian coordinates:

$$Y_{2,0}^*(\Theta, \Phi) = \frac{1}{2} \sqrt{\frac{5}{4\pi}} Q_{33} \frac{1}{R^2} \quad (\text{A.10})$$

$$Y_{2,\pm 1}^*(\Theta, \Phi) = \mp \frac{1}{6} \sqrt{\frac{15}{8\pi}} (2Q_{13} \mp 2iQ_{23}) \frac{1}{R^2} \quad (\text{A.11})$$

$$Y_{2,\pm 2}^*(\Theta, \Phi) = \mp \frac{1}{12} \sqrt{\frac{15}{2\pi}} (Q_{11} \pm 2iQ_{12} - Q_{22}) \frac{1}{R^2} \quad (\text{A.12})$$

where

$$Q_{ij} = 3x_i x_j - \delta_{ij} R^2$$

We can see from this that

$$\begin{aligned} \frac{Q_{ij}}{R^5} &= \frac{3(\hat{n}_i \cdot \vec{R})(\hat{n}_j \cdot \vec{R})}{R^5} - \frac{\hat{n}_i \cdot \hat{n}_j}{R^3} \\ &= (\hat{n}_i \cdot \vec{\nabla}_\epsilon)(\hat{n}_j \cdot \vec{\nabla}_\epsilon) \left[\frac{1}{|\vec{R} - \vec{\epsilon}|} \right]_{\epsilon=0} \end{aligned} \quad (\text{A.13})$$

So substituting the Ewald sum and taking the required derivatives, we get[46]:

$$\begin{aligned} \sum_{\vec{R}} Q_{ij} &= -\frac{4\pi}{v_c} \sum_{\vec{K} \neq 0} G_{ij}(\vec{K}) e^{-K^2/4g^2 + i\vec{K} \cdot \vec{d}} \\ &\quad + \sum_{\vec{R} \neq 0} [S1_{ij}(\vec{d} - \vec{R}) - S2_{ij}(\vec{d} - \vec{R})] \\ &\quad - Y_{ij} \end{aligned} \quad (\text{A.14})$$

where

$$G_{ij}(\vec{K}) = \frac{K_i K_j}{K^2} \quad (\text{A.15})$$

$$S1_{ij}(\vec{R}) = \delta_{ij} \left(\frac{2g}{\sqrt{pi}} \frac{e^{-g^2 R^2}}{R^2} + \frac{\text{erfc}(g|\vec{R}|)}{R^3} \right) \quad (\text{A.16})$$

$$S2_{ij}(\vec{R}) = R_i R_j \left(\left[\frac{4g^3}{\sqrt{\pi} R^2} + \frac{6g}{\sqrt{\pi} R^4} \right] + \frac{3\text{erfc}(g|\vec{R}|)}{R^5} \right) \quad (\text{A.17})$$

$$Y_{ij} = -\frac{\delta_{ij}}{d^3} + \frac{3R_i R_j}{d^5} + S1_{ij}(\vec{d}) - S2_{ij}(\vec{d}) \quad (\text{A.18})$$

We also note here that in the limiting case $\vec{d} \rightarrow 0$,

$$Y_{ij} = -\frac{4g^3}{3\sqrt{\pi}} \delta_{ij}$$

These terms are relatively easy to compute since many of the factors needed are already calculated and stored for computing the $l = 0$ term. For the $l = 4$ terms, since the terms have a factor of R^5 in them, the individual sublattices are absolutely convergent. Thus these terms can be evaluated without modification for each sublattice.

The last piece necessary for the crystal field calculation is the radial expectation values, $\langle r^2 \rangle$ and $\langle r^4 \rangle$. These were calculated from ref [30], using Rootham-Hartree-Fock atomic wavefunctions.

Appendix B

Detailed Ground State Information

B.1 NiO

```
//Program input
XCRD:
(
// XAS calculation Ni d8
Dq=1.0; // 10Dq value
pds=1.7; // hopping parameters
pdp=-pds/2.2;
Udd=6.0; // d-d Coulomb repulsion value
Dt=5.0; // Charge transfer energy
// Slater Integrals for multiplet structure
F2dd=10.45;
F4dd=7.35;
F2pd=7.72;
G1pd=5.79;
G3pd=3.29;
// Spin-orbit coupling
```

```
xi=11.3464;
)
// Initial and Final Configurations considered
CNFG:
      2p  3d  Ld
#i1  6   8   10
#i2  6   9   9
#i3  6  10   8

#f1  5   9   10
#f2  5  10   9

XEND:
STOP:

=====
Xtls ver. 8.30 coded by Arata Tanaka on 6th Sep. 2004
compiled for scaler machine
===== state #i =====
#           1   E=  -3.04247780890822
-----

Orbit ==> 3d
Sx=  0.1166654      Sy=  0.000000      Sz= -0.4938412
Lx= -0.8772830E-16 Ly=  0.000000      Lz=  0.7216450E-15
Mx= -0.2333309      My=  0.000000      Mz=  0.9876824
Tx=  0.1897787E-14 Ty=  0.000000      Tz= -0.3903128E-16

S^2=  1.869639
SySz+SzSy=  0.000000      SzSx+SxSz= -0.3700758
SxSy+SySx=  0.000000
3Sx^2-S^2= -1.453095      3Sy^2-S^2=  0.6875516
```

$3S_z^2 - S^2 = 0.7655436$
 $S_y^2 - S_z^2 = -0.2599735E-01$ $S_z^2 - S_x^2 = 0.7395463$
 $S_x^2 - S_y^2 = -0.7135489$

 $L^2 = 11.37038$
 $L_y L_z + L_z L_y = 0.000000$ $L_z L_x + L_x L_z = 0.2394014E-14$
 $L_x L_y + L_y L_x = 0.000000$
 $3L_x^2 - L^2 = 0.4301499E-14$ $3L_y^2 - L^2 = 0.1915750E-14$
 $3L_z^2 - L^2 = -0.6217249E-14$
 $L_y^2 - L_z^2 = 0.2711000E-14$ $L_z^2 - L_x^2 = -0.3506249E-14$
 $L_x^2 - L_y^2 = 0.7952495E-15$

$J^2 = 13.24002$
 $J_y J_z + J_z J_y = 0.000000$ $J_z J_x + J_x J_z = -0.3700758$
 $J_x J_y + J_y J_x = 0.000000$
 $3J_x^2 - J^2 = -1.453095$ $3J_y^2 - J^2 = 0.6875516$
 $3J_z^2 - J^2 = 0.7655436$
 $J_y^2 - J_z^2 = -0.2599735E-01$ $J_z^2 - J_x^2 = 0.7395463$
 $J_x^2 - J_y^2 = -0.7135489$

Orbit ==> ld

$S_x = 0.6460210E-02$ $S_y = 0.000000$ $S_z = -0.2734587E-01$
 $L_x = -0.5015432E-15$ $L_y = 0.000000$ $L_z = -0.2411482E-14$
 $M_x = -0.1292042E-01$ $M_y = 0.000000$ $M_z = 0.5469174E-01$
 $T_x = -0.1093019E-14$ $T_y = 0.000000$ $T_z = -0.1180821E-15$

$S^2 = 0.7951315E-01$
 $S_y S_z + S_z S_y = 0.000000$ $S_z S_x + S_x S_z = -0.6690080E-03$
 $S_x S_y + S_y S_x = 0.000000$
 $3S_x^2 - S^2 = -0.2626846E-02$ $3S_y^2 - S^2 = 0.1242928E-02$
 $3S_z^2 - S^2 = 0.1383918E-02$

Sy²-Sz²= -0.4699695E-04 Sz²-Sx²= 0.1336922E-02
 Sx²-Sy²= -0.1289925E-02

L²= 0.6296212

LyLz+LzLy= 0.000000 LzLx+LxLz= 0.4247138E-14

LxLy+LyLx= 0.000000

3Lx²-L²= -0.4967632E-14 3Ly²-L²= -0.2581884E-14

3Lz²-L²= 0.7549517E-14

Ly²-Lz²= -0.3377134E-14 Lz²-Lx²= 0.4172383E-14

Lx²-Ly²= -0.7952495E-15

J²= 0.7091344

JyJz+JzJy= 0.000000 JzJx+JxJz= -0.6690080E-03

JxJy+JyJx= 0.000000

3Jx²-J²= -0.2626846E-02 3Jy²-J²= 0.1242928E-02

3Jz²-J²= 0.1383918E-02

Jy²-Jz²= -0.4699695E-04 Jz²-Jx²= 0.1336922E-02

Jx²-Jy²= -0.1289925E-02

 Orbit #1 ==>3d Orbit #2 ==>1d

<S₂ S₁>= 0.2542372E-01 <L₂ L₁>= -0.1133656E-26

<J₂ J₁>= 0.2542372E-01

 Total moments over the orbitals specified in "Mag" command.

<S₂ S₁>= 2.000000 <L₂ L₁>= 12.00000

<J₂ J₁>= 14.00000

----- configuration mixing -----

#	1	E=	-3.04247780890822	
CI=#i1			89.6684119497364	%
CI=#i2			10.1694891533274	%

CI=#i3 0.162098896936246 %

===== state #i =====

1 E= -3.04247780890822

C4 -0.0488 0.5212

C3 0.2134 0.2257

C2 -0.9025 0.0000

Orbit => 3d

----- electron occupation -----

m	down	up		down	up	Jz	J=3/2	J=5/2
2	0.8866	0.6397	Eg u	0.7732	0.2793	5/2		0.6397
1	1.0000	1.0000	Eg v	0.7732	0.2793	3/2	0.9093	0.9773
0	0.7732	0.2793	T2g a	1.0000	1.0000	1/2	0.7117	0.5676
-1	1.0000	1.0000	T2g b	1.0000	1.0000	-1/2	0.9093	0.8639
-2	0.8866	0.6397	T2g c	1.0000	1.0000	-3/2	0.7117	0.9279
sum	4.5463	3.5586				-5/2		0.8866
total	8.1049							

Orbit => 1d

----- electron occupation -----

m	down	up		down	up	Jz	J=3/2	J=5/2
2	0.9937	0.9800	Eg u	0.9874	0.9601	5/2		0.9800
1	1.0000	1.0000	Eg v	0.9874	0.9601	3/2	0.9950	0.9987
0	0.9874	0.9601	T2g a	1.0000	1.0000	1/2	0.9840	0.9761
-1	1.0000	1.0000	T2g b	1.0000	1.0000	-1/2	0.9950	0.9925
-2	0.9937	0.9800	T2g c	1.0000	1.0000	-3/2	0.9840	0.9960
sum	4.9749	4.9202				-5/2		0.9937
total	9.8951							

B.2 NaNiO₂

XCRD:

```
(  
// Input of Parameters  
  
// parameters we can vary  
Dq=1.5; \\ Crystal Field splitting  
pds=1.7; \\ hopping term  
Jt=0.737158; \\ Jahn-Teller splitting  
Udd=6.0; \\ d-d Coulomb repulsion  
Dt=13.1894; \\ Charge Transfer Energy  
xi=11.8917; \\ spin-orbit coupling  
  
// Slater integrals for the multiplet terms  
F2dd=10.45;  
F4dd=7.35;  
F2pd=7.72;  
G1pd=5.79;  
G3pd=3.29;  
  
// Configurations considered  
CNFG:  
    2p  3d  Ld  
#i1  6   7  10  
#i2  6   8   9  
#i3  6   9   8  
#i4  6  10   7  
  
#f1  5   8  10  
#f2  5   9   9
```

#f3 5 10 8

XEND:

STOP:

// Program Output

=====

Xtls ver. 8.30 coded by Arata Tanaka on 6th Sep. 2004

compiled for scaler machine

===== state #i =====

1 E= -5.92893328355149

Orbit ==> 3d

Sx=	0.6675136E-01	Sy=	0.000000	Sz=	-0.4616470
Lx=	0.1963538E-15	Ly=	0.000000	Lz=	0.2220446E-15
Mx=	-0.1335027	My=	0.000000	Mz=	0.9232939
Tx=	-0.1851441E-01	Ty=	0.000000	Tz=	-0.2560883

S²= 0.8282715

SySz+SzSy= 0.000000 SzSx+SxSz= 0.3747003E-15

SxSy+SySx= 0.000000

3Sx²-S²= 0.4516615E-15 3Sy²-S²= -0.8957507E-15

3Sz²-S²= 0.4440892E-15

Sy²-Sz²= -0.4466133E-15 Sz²-Sx²= -0.2524106E-17

Sx²-Sy²= 0.4491374E-15

L²= 17.37453

LyLz+LzLy= 0.000000 LzLx+LxLz= 0.2513098E-13

LxLy+LyLx= 0.000000

3Lx²-L²= 3.155956 3Ly²-L²= 3.155956

3Lz²-L²= -6.311911

Ly²-Lz²= 3.155956 Lz²-Lx²= -3.155956

$$L_x^2 - L_y^2 = -0.1487656E-14$$

$$J^2 = 18.20280$$

$$J_y J_z + J_z J_y = 0.000000 \quad J_z J_x + J_x J_z = 0.2831763E-13$$

$$J_x J_y + J_y J_x = 0.000000$$

$$3J_x^2 - J^2 = 3.155956 \quad 3J_y^2 - J^2 = 3.155956$$

$$3J_z^2 - J^2 = -6.311911$$

$$J_y^2 - J_z^2 = 3.155956 \quad J_z^2 - J_x^2 = -3.155956$$

$$J_x^2 - J_y^2 = 0.2287661E-13$$

Orbit ==> ld

$$S_x = 0.4801495E-02 \quad S_y = 0.000000 \quad S_z = -0.3320675E-01$$

$$L_x = 0.1076291E-14 \quad L_y = 0.000000 \quad L_z = -0.9366423E-15$$

$$M_x = -0.9602990E-02 \quad M_y = 0.000000 \quad M_z = 0.6641350E-01$$

$$T_x = -0.1841115E-02 \quad T_y = 0.000000 \quad T_z = -0.2546600E-01$$

$$S^2 = 0.1789278$$

$$S_y S_z + S_z S_y = 0.000000 \quad S_z S_x + S_x S_z = -0.1214306E-15$$

$$S_x S_y + S_y S_x = 0.000000$$

$$3S_x^2 - S^2 = 0.6043975E-15 \quad 3S_y^2 - S^2 = 0.8949193E-16$$

$$3S_z^2 - S^2 = -0.6938894E-15$$

$$S_y^2 - S_z^2 = 0.2611271E-15 \quad S_z^2 - S_x^2 = -0.4327623E-15$$

$$S_x^2 - S_y^2 = 0.1716352E-15$$

$$L^2 = 1.486426$$

$$L_y L_z + L_z L_y = 0.000000 \quad L_z L_x + L_x L_z = -0.3269041E-14$$

$$L_x L_y + L_y L_x = 0.000000$$

$$3L_x^2 - L^2 = 0.2698729 \quad 3L_y^2 - L^2 = 0.2698729$$

$$3L_z^2 - L^2 = -0.5397459$$

$$L_y^2 - L_z^2 = 0.2698729 \quad L_z^2 - L_x^2 = -0.2698729$$

$$L_x^2 - L_y^2 = 0.2058267E-14$$

```

J^2= 1.665353
JyJz+JzJy= 0.000000      JzJx+JxJz= -0.5336443E-14
JxJy+JyJx= 0.000000
3Jx^2-J^2= 0.2698729      3Jy^2-J^2= 0.2698729
3Jz^2-J^2= -0.5397459
Jy^2-Jz^2= 0.2698729      Jz^2-Jx^2= -0.2698729
Jx^2-Jy^2= 0.8587339E-16

```

```

-----
Orbit #1 ==>3d      Orbit #2 ==>ld
<S_2 S_1>= -0.1285996      <L_2 L_1>= -0.3683474E-01
<J_2 J_1>= -0.1654344

```

```

-----
Total moments over the orbitals specified in "Mag" command.
<S_2 S_1>= 0.7500000      <L_2 L_1>= 18.78729
<J_2 J_1>= 19.53729

```

```

----- configuration mixing -----
#           1      E= -5.92893328355149
CI=#i1           76.5349337915624      %
CI=#i2           22.1876328190364      %
CI=#i3           1.26162666914198      %
CI=#i4           1.580672025926590E-002 %

```

```

===== state #i =====
#           1      E= -5.92893328355149
C4 -0.7071  0.6998
C3 -0.2499  0.4284
C2 0.0000 -0.9897
Orbit => 3d

```

```

----- electron occupation -----

```

m	down	up		down	up	Jz	J=3/2	J=5/2
2	0.9932	0.5383	Eg u	0.1071	0.0939	5/2		0.5383
1	0.9960	0.9958	Eg v	0.9946	0.0848	3/2	0.9937	0.9953
0	0.1071	0.0939	T2g a	0.9960	0.9958	1/2	0.6352	0.4547
-1	0.9960	0.9958	T2g b	0.9960	0.9958	-1/2	0.6403	0.4626
-2	0.9932	0.5383	T2g c	0.9917	0.9918	-3/2	0.6298	0.9045
sum	4.0854	3.1621				-5/2		0.9932
total	7.2476							
Orbit => ld								

----- electron occupation -----

m	down	up		down	up	Jz	J=3/2	J=5/2
2	0.9997	0.9608	Eg u	0.9101	0.9214	5/2		0.9608
1	0.9999	0.9999	Eg v	0.9996	0.9218	3/2	0.9998	0.9999
0	0.9101	0.9214	T2g a	0.9999	0.9999	1/2	0.9685	0.9528
-1	0.9999	0.9999	T2g b	0.9999	0.9999	-1/2	0.9640	0.9460
-2	0.9997	0.9608	T2g c	0.9999	0.9999	-3/2	0.9687	0.9921
sum	4.9094	4.8430				-5/2		0.9997
total	9.7524							

B.3 LiNiO₂

XCRD:

```
(
// Input of parameters

// parameters we can vary
Dq=0.69047; // Splitting on the Ni site
LDq=-0.570614; // Splitting on the ligand site
pds=1.95434; // hopping parameters
pdp=-1.25228;
```

```
Udd=5.98116; // d-d Coulomb repulsion
Dt=5.58655; // Charge transfer energy
xi=11.4922; // Spin orbit coupling

// various Slater integrals
F2dd=10.45;
F4dd=7.35;
F2pd=7.72;
G1pd=5.79;
G3pd=3.29;
)
// configurations considered
CNFG:
      2p  3d  Ld
#i1  6   7  10
#i2  6   8   9
#i3  6   9   8
#i4  6  10   7

#f1  5   8  10
#f2  5   9   9
#f3  5  10   8

// Program Output
=====
Xtls ver. 8.30 coded by Arata Tanaka on 6th Sep. 2004
compiled for scaler machine
===== state #i =====
#           1   E= -8.88102034735880
-----
Orbit ==> 3d
```

MSc Thesis - E. A. Mills - McMaster - Dept of Physics & Astronomy

Sx= 0.1427638 Sy= 0.000000 Sz= -0.2478559
 Lx= -0.1021206E-14 Ly= 0.000000 Lz= 0.1332268E-14
 Mx= -0.2855276 My= 0.000000 Mz= 0.4957117
 Tx= 0.1633857 Ty= 0.000000 Tz= -0.1255188

S²= 1.034803
 SySz+SzSy= 0.000000 SzSx+SxSz= -0.8326673E-16
 SxSy+SySx= 0.000000
 3Sx²-S²= -0.2164664E-15 3Sy²-S²= 0.1326689E-14
 3Sz²-S²= -0.1110223E-14
 Sy²-Sz²= 0.8123041E-15 Sz²-Sx²= -0.2979189E-15
 Sx²-Sy²= -0.5143853E-15

L²= 13.36334
 LyLz+LzLy= 0.000000 LzLx+LxLz= 0.2829920E-14
 LxLy+LyLx= 0.000000
 3Lx²-L²= -1.836756 3Ly²-L²= 2.702426
 3Lz²-L²= -0.8656700
 Ly²-Lz²= 1.189365 Lz²-Lx²= 0.3236952
 Lx²-Ly²= -1.513060

J²= 14.39814
 JyJz+JzJy= 0.000000 JzJx+JxJz= 0.4385381E-14
 JxJy+JyJx= 0.000000
 3Jx²-J²= -1.836756 3Jy²-J²= 2.702426
 3Jz²-J²= -0.8656700
 Jy²-Jz²= 1.189365 Jz²-Jx²= 0.3236952
 Jx²-Jy²= -1.513060

Orbit ==> ld

Sx= 0.2942500E-01 Sy= 0.000000 Sz= -0.5108550E-01

Lx= -0.8913140E-15 Ly= 0.000000 Lz= -0.1623249E-15
Mx= -0.5885001E-01 My= 0.000000 Mz= 0.1021710
Tx= 0.6202720E-01 Ty= 0.000000 Tz= -0.4765155E-01

S²= 0.5411346

SySz+SzSy= 0.000000 SzSx+SxSz= 0.5204170E-17

SxSy+SySx= 0.000000

3Sx²-S²= -0.8126534E-16 3Sy²-S²= -0.1962904E-15

3Sz²-S²= 0.2775558E-15

Sy²-Sz²= -0.1579487E-15 Sz²-Sx²= 0.1196070E-15

Sx²-Sy²= 0.3834169E-16

L²= 5.184696

LyLz+LzLy= 0.000000 LzLx+LxLz= 0.2913931E-15

LxLy+LyLx= 0.000000

3Lx²-L²= -1.142068 3Ly²-L²= 1.680329

3Lz²-L²= -0.5382611

Ly²-Lz²= 0.7395302 Lz²-Lx²= 0.2012690

Lx²-Ly²= -0.9407992

J²= 5.725831

JyJz+JzJy= 0.000000 JzJx+JxJz= -0.2740863E-14

JxJy+JyJx= 0.000000

3Jx²-J²= -1.142068 3Jy²-J²= 1.680329

3Jz²-J²= -0.5382611

Jy²-Jz²= 0.7395302 Jz²-Jx²= 0.2012690

Jx²-Jy²= -0.9407992

Orbit #1 ==>3d Orbit #2 ==>1d
<S_2 S_1>= -0.4129686 <L_2 L_1>= -0.2408502
<J_2 J_1>= -0.6538188

 Total moments over the orbitals specified in "Mag" command.

<S_2 S_1>= 0.7500000 <L_2 L_1>= 18.06634
 <J_2 J_1>= 18.81634

----- configuration mixing -----

#	1	E=	-8.88102034735880	
CI=#i1			30.1088046881058	%
CI=#i2			54.8112683537870	%
CI=#i3			14.3896516200227	%
CI=#i4			0.690275338084464	%

===== state #i =====

#	1	E=	-8.88102034735880
C4	-0.1530	0.4348	
C3	-0.1029	0.2637	
C2	0.0000	-0.5979	

Orbit => 3d

----- electron occupation -----

m	down	up		down	up	Jz	J=3/2	J=5/2
2	0.8649	0.6312	Eg u	0.4556	0.4277	5/2		0.6312
1	0.9953	0.9951	Eg v	0.7355	0.2681	3/2	0.8910	0.9691
0	0.4556	0.4277	T2g a	0.9937	0.9936	1/2	0.7683	0.6548
-1	0.9953	0.9951	T2g b	0.9970	0.9967	-1/2	0.7793	0.6714
-2	0.8649	0.6312	T2g c	0.9943	0.9943	-3/2	0.7040	0.9225
sum	4.1762	3.6805				-5/2		0.8649
total	7.8566							

Orbit => 1d

----- electron occupation -----

m	down	up		down	up	Jz	J=3/2	J=5/2
2	0.9378	0.8705	Eg u	0.7490	0.7813	5/2		0.8705

MSc Thesis - E. A. Mills - McMaster - Dept of Physics & Astronomy

1	0.9991	0.9991	Eg v	0.8766	0.7420	3/2	0.9500	0.9869
0	0.7490	0.7813	T2g a	0.9988	0.9989	1/2	0.9120	0.8684
-1	0.9991	0.9991	T2g b	0.9994	0.9994	-1/2	0.8991	0.8491
-2	0.9378	0.8705	T2g c	0.9989	0.9990	-3/2	0.8962	0.9734
sum	4.6228	4.5206				-5/2		0.9378
total	9.1434							

Bibliography

- [1] E. Chappel, M.D. Nunez-Regueiro, G. Chouteau, O. Isnard, and C. Darie. Study of the ferrodistorptive orbital ordering in nanio[_{sub} 2] by neutron diffraction and submillimeter wave esr. *Eur Phys J B*, 17:615–622, 2000.
- [2] M. Holzapfel, S. de Brion, C. Darie, P. Bordet, E. Chappel, G. Chouteau, P. Strobel, A. Sulpice, and M. D. Núñez Regueiro. Decoupling of orbital and spin degrees of freedom in $li_{1-x}n_xnio_2$. *Phys Rev B*, 70(13):132410, Oct 2004.
- [3] M. A. van Veenendaal and G. A. Sawatzky. Doping dependence of $ni2p$ x-ray-absorption spectra of m_xni_{1-x} ($m = li, na$). *Phys Rev B*, 50(16):11326–11331, Oct 1994.
- [4] P. Kuiper, G. Kruizinga, J. Ghijsen, and G. A. Sawatzky. Character of holes in $li_2ni_{1-x}o$ and their magnetic behavior. *Phys Rev Lett*, 62(2):221–224, 1989.
- [5] J. van Elp, H. Eskes, P. Kuiper, and G. A. Sawatzky. Electronic structure of li-doped nio. *Phys Rev B*, 45(4):1612–1622, Jan 1992.
- [6] L. A. Montoro, M. Abbate, E. C. Almeida, and J. M. Rosolen. Electronic structure of the transition metal ions in $licoo_2$, $linio_2$, and $lico_{0.5}ni_{0.5}o_2$. *Chem Phys Lett*, 309:14–18, 1999.
- [7] E. Chappel, M.D. Nunez-Regueiro, F. Dupont, G. Chouteau, C. Darie, and A. Sulpice. Antiferromagnetic resonance and high magnetic field properties of nanio[_{sub} 2]. *Eur Phys J B*, 17:609–914, 2000.

- [8] M. J. Lewis, B. D. Gaulin, L. Filion, C. Kallin, A. J. Berlinsky, H. A. Dabkowska, Y. Qiu, and J. R. D. Copley. Ordering and spin waves in nio₂: A stacked quantum ferromagnet. *Phys Rev B*, 72(1):014408, 2005.
- [9] M. V. Mostovoy and D. I. Khomskii. Orbital ordering in frustrated jahn-teller systems with 90 deg exchange. *Phys Rev Lett*, 89(22):227203, Nov 2002.
- [10] P. W. Anderson. Resonating valence bonds: A new kind of insulator? *Mater Res Bull*, 8(2):153–160, 1973.
- [11] K. Hirakawa, H. Kadowaki, and K. Ubukoshi. Experimental studies of triangular lattice antiferromagnets with $s = 1/2$: Nio₂ and lino₂. *J Phys Soc Jap*, 54(9):3526–3536, 1985.
- [12] K. Hirakawa, R. Osborn, A. D. Taylor, and K. Takeda. Neutron inelastic scattering study of lino₂: a candidate for the spin quantum liquid. *J Phys Soc Jap*, 59(9):3081–3084, 1990.
- [13] H. Yoshizawa, H. Mori, K. Hirota, and M. Ishikawa. Ferromagnetic short-range correlations in a two-dimensional triangular lattice antiferromagnet with $s = 1/2$ lino₂. *J Phys Soc Jap*, 59(8):2631–2634, 1990.
- [14] K. Hirota, Y. Nakazawa, and M. Ishikawa. Magnetic properties of the $s = 1/2$ antiferromagnetic triangular lattice lino₂. *J Phys: Condens Matter*, 3:4721–4730, 1991.
- [15] J. N. Reimers, J. R. Dahn, J. E. Greedan, C. V. Stager, G. Liu, I. Davidson, and U. von Sacken. Spin glass behavior in the frustrated antiferromagnetic lino₂. *J Solid State Chem*, 102:542–552, 1993.
- [16] M. D. Núñez Regueiro, E. Chappel, G. Chouteau, and C. Delmas. Magnetic structure of $li_{1-x}ni_{1+x}o_2$. *Eur Phys J B*, 16:37–41, 2000.

- [17] Y. *et al* Kitaoka. Orbital frustration and resonating valence bond state in the spin-1/2 triangular lattice LiNiO_2 . *J Phys Soc Jap*, 67(11):3703–3706, 1998.
- [18] F. Reynaud, D. Mertz, F. Celestini, J.-M. Debierre, A. M. Ghorayeb, P. Simon, A. Stepanov, J. Voiron, and C. Delmas. Orbital frustration at the origin of the magnetic behavior in LiNiO_2 . *Phys Rev Lett*, 86(16):3638–3641, Apr 2001.
- [19] A.-M. Dare, R. Hayn, and J.-L. Richard. Orbital and spin exchange in LiNiO_2 . *Europhysics Letters*, 61:803–809, 2003.
- [20] Karlo Penc, Matthieu Mambrini, Patrik Fazekas, and Frédéric Mila. Quantum phase transition in the $\text{su}(4)$ spin-orbital model on the triangular lattice. *Phys Rev B*, 68(1):012408, Jul 2003.
- [21] F. Vernay, K. Penc, P. Fazekas, and F. Mila. Orbital degeneracy as a source of frustration in LiNiO_2 . *Phys Rev B*, 70(1):014428, Jul 2004.
- [22] J.-S. Kang, S. S. Lee, G. Kim, H. J. Lee, H. K. Song, Y. J. Shin, S. W. Han, C. Hwang, M. C. Jung, H. J. Shin, B. H. Kim, S. K. Kwon, and B. I. Min. Valence and spin states in delafossite LiNiO_2 and the frustrated jahn-teller system LiNiO_2 ($a=\text{Li,Na}$). *Phys Rev B*, 76:195122, 2007.
- [23] A. Tanaka and T. Jo. Resonant $3d$, $3p$, and $3s$ photoemission in transition metal oxides predicted at $2p$ threshold. *J Phys Soc Jap*, 63(7):2788–2807, 1994.
- [24] N. F. Mott. *Proc Phys Soc, London, Sect A*, 62:416, 1949.
- [25] J.-H. Chung, Th. Proffen, S. Shamoto, A. M. Ghorayeb, L. Croguennec, W. Tian, B. C. Sales, R. Jin, D. Mandrus, and T. Egami. Local structure of LiNiO_2 studied by neutron diffraction. *Phys Rev B*, 71(6):064410, 2005.

- [26] S. Eisebitt, T. Bske, J.-E. Rubensson, and W. Eberhardt. Determination of absorption coefficients for concentrated samples by fluorescence detection. *Phys Rev B*, 47(21):14103–14109, 1993.
- [27] B.L. Henke, E.M. Gullikson, and J.C. Davis. *Atomic Data and Nuclear Data Tables*, 54:181, 1993.
- [28] H. Ehrenreich, F. Seitz, and D. Turnbull, editors. *Solid State Physics*, volume 35. Academic Press, 1980.
- [29] M. Abramowitz and I. A. Stegun. *Handbook of Mathematical Functions, with Formulas, Graphs, and Mathematical Tables*. Dover New York, 1965.
- [30] E. Clementi and C. Roetti. *Atomic Data and Nuclear Data Tables*, 14:177–478, 1974.
- [31] S. V. Streltsov, A. S. Mylnikova, A. O. Shorikov, Z. V. Pchelkina, D. I. Khomskii, and V. I. Anisimov. Crystal-field splitting for low symmetry systems in ab initio calculations. *Phys Rev B*, 71(24):245114, 2005.
- [32] M. Tinkham. *Group Theory and Quantum Mechanics*. McGraw-Hill New York, 1964.
- [33] J. C. Slater and G. F. Koster. Simplified lcao method for the periodic potential problem. *Physical Review*, 94:1498–1524, 1954.
- [34] J. C. Slater. *Quantum Theory of Atomic Structure*, volume 1. McGraw-Hill New York, 1960.
- [35] Robert Schmitz, Ora Entin-Wohlman, Amnon Aharony, A. Brooks Harris, and Erwin Muller-Hartmann. Magnetic structure of the jahn-teller system LaTiO_3 . *Phys Rev B*, 71(14):144412, 2005.
- [36] A. E. Bocquet, T. Mizokawa, T. Saitoh, H. Namatame, and A. Fujimori. Electronic structure of 3d-transition-metal compounds by analysis of the 2p core-level photoemission spectra. *Phys Rev B*, 46:3771, 1992.

- [37] J. J. Sakurai. *Modern Quantum Mechanics*. Addison Wesley, 1994.
- [38] J. Kanamori and A. Kotani, editors. *Core-Level Spectroscopy in Condensed Matter Systems*. Springer-Verlag, 1988.
- [39] G. van der Laan, J. Zaanen, G. A. Sawatzky, R. Karnatak, and J.-M. Esteve. Comparison of x-ray absorption with x-ray photoemission of nickel dihalides and nio. *Phys Rev B*, 33(6):4253–4263, Mar 1986.
- [40] T. Mizokawa, A. Fujimori, T. Arima, Y. Tokura, N. Mori, and J. Akimitsu. Electronic structure of prnio_3 studied by photoemission and x-ray absorption spectroscopy: Band gap and orbital ordering. *Phys Rev B*, 52:13865, 1995.
- [41] F. M. F. de Groot. *J Elec Spect and Rel Phenom*, 67:529–622, 1994.
- [42] J. M. Ziman. *Principles of the Theory of Solids*. Cambridge University Press, 1972.
- [43] M. P. Marder. *Condensed Matter Physics*. John Wiley New York, 2000.
- [44] J. W. Perram, H. G. Peterson, and S. W. de Leeuw. *Molec Phys*, 65:875–893, 1988.
- [45] J. Kolafa and J. W. Perram. *Molec Simulation*, 9:351–368, 1992.
- [46] Matthew Enjalran and Michel J. P. Gingras. Theory of paramagnetic scattering in highly frustrated magnets with long-range dipole-dipole interactions: The case of the $\text{tb}_2\text{ti}_2\text{o}_7$ pyrochlore antiferromagnet. *Phys Rev B*, 70(17):174426, Nov 2004.

